

## IMMUNOLOGY

# Lymph node–targeted DNA engages TBK1/IFN-I–driven innate immunity to induce potent T cell responses and durable memory in mice and NHPs

Martin P. Steinbuck<sup>1</sup>, Lochana M. Seenappa<sup>1</sup>, Wei Zhan<sup>2</sup>, Erica Palmer<sup>1</sup>, Mimi M. Jung<sup>1</sup>, Anieli Jakubowski<sup>1</sup>, Xavier Cabana-Puig<sup>1</sup>, Lisa K. McNeil<sup>1</sup>, Christopher M. Haqq<sup>1</sup>, Katherine A. Fitzgerald<sup>2</sup>, Peter C. DeMuth<sup>1\*</sup>

Adjuvants are immunoactivators capable of shaping the magnitude and quality of antigen-specific immune responses induced by subunit immunization. Presently, there is an acute need for effective adjuvants that safely induce durable and balanced humoral and cellular responses. Here, we engineered a class of Amphiphile (AMP)–modified, immunostimulatory DNA adjuvants designed for targeted delivery to lymph nodes and enhanced stimulation of TANK-binding kinase 1 (TBK1)–mediated danger-sensing pathways to generate strong adaptive immunity and long-term memory with potent recall potential. AMP-DNA adjuvants induced robust interferon type-I (IFN-I)–driven inflammatory environments in mouse and nonhuman primate (NHP) lymph nodes, leading to significantly enhanced cytokine secretion by polyfunctional CD8<sup>+</sup> and CD4<sup>+</sup> T cells in multiple tissues, as well as strongly elevated T helper cell 1 (T<sub>H</sub>1)–associated and neutralizing antibody responses, in the absence of systemic toxicity. These results demonstrate that AMP modification enables lymph node–targeted DNA adjuvants to potentially activate IFN-I signaling to generate substantial cellular and humoral responses crucial for vaccine efficacy.

## INTRODUCTION

Vaccines have transformed public health since their inception and remain one of the most cost-effective and widely applied health interventions available. At present, modern protein subunit vaccines use highly defined antigens to elicit precise and safe immune responses against their specific targets. However, such refined antigens, in isolation, often lack ancillary immunostimulatory elements that engage the innate immune system to induce robust and lasting immunity. Thus, besides a few exceptions (1, 2), adjuvants have become indispensable components of subunit vaccines essential for stimulating adequate responses to target antigens (3). Whereas some adjuvants can operate as antigen delivery or depot systems, others mainly work as immunostimulants that activate antigen-presenting cells (APCs) through Toll-like receptors (TLRs) or other pattern recognition receptors (PRRs) (4). To date, the most commonly used adjuvants in commercially available prophylactic vaccines are the aluminum phosphate salt alum and the oil-in-water emulsion MF59 (5). Notable disadvantages of these classical adjuvants often include the lack of long-term protective immunity (4, 6) and a poor ability to induce cellular immune responses (7) critical for protection against intracellular pathogens such as malaria (8, 9), tuberculosis (10, 11), and viruses, as well as cancer (12). In contrast, many molecular adjuvants, including TLR agonists, are promising adjuvant candidates as they often stimulate interferon type-I (IFN-I) and inflammatory cytokine responses, which have the potential to induce strong cellular immunity (4). Nonetheless, only a small number of these immunostimulatory PRR agonists have been tested in clinical trials and approved for use in humans, including synthetic double-stranded RNA [e.g., polyinosinic:polycytidylic acid [poly(I:C)]/poly-ICLC, a TLR3 agonist], oligodeoxynucleotides (ODNs; e.g., CpG-7909, a TLR9 agonist), cyclic dinucleotides [e.g., cyclic guanosine monophosphate and

adenosine monophosphate (cGAMP), a stimulator of interferon genes (STING) agonist], and nucleoside analogs (e.g., resiquimod, a TLR7/8 agonist), with only CpG ODNs having been licensed for commercial use in the US. A common obstacle with molecular adjuvants is their tendency to either remain in the injection site (molecules >100 kDa) or be distributed systemically (<20 kDa), as low-molecular weight compounds readily diffuse into circulation through capillary endothelial tight junctions (13). This often leads to rapid systemic dissemination toward potentially immunologically irrelevant or tolerizing sites. Systemic exposure of adjuvants thus makes it difficult to achieve sufficient immunostimulation while avoiding reactogenicity, necessitating dose restrictions, which limit their use in practice (14–16).

However, recent innovations in adjuvant design and the use of delivery platforms including the saponin-based formulations AS01 and Matrix-M, as well as other engineered nanoparticles, have contributed to increased adjuvant activity, vaccine immunogenicity, and improved safety (17–19). Among these efforts are technologies that aim to enhance the biodistribution and thus potency of vaccines by targeting delivery directly to lymph nodes (LNs), where protective immune responses are coordinated (20). One such approach is “albumin-hitchhiking,” which uses albumin’s size-dependent (~65 kDa) migration through the lymphatics, to accumulate vaccines in draining LNs (21, 22). The resulting targeted bioavailability and increased APC uptake of antigens and adjuvants consequently initiate robust adaptive immune responses. Accordingly, to allow for transient association with albumin, antigens and adjuvants can be chemically modified with albumin-binding moieties (23–25). We have particularly focused on the preclinical and clinical development of amphiphilic lipid polymer [Amphiphile (AMP)] conjugates, wherein a molecular payload of interest is linked to an albumin-binding phospholipid tail, enabling noncovalent association with endogenous albumin following injection into tissue that mediates efficient targeting to draining LNs via the lymphatics. AMP conjugates have previously been demonstrated in mice and nonhuman primates (NHPs) to

<sup>1</sup>Elicio Therapeutics, 451 D Street, 5th Floor, Suite 501, Boston, MA 02210, USA.

<sup>2</sup>Program in Innate Immunity, Department of Medicine, University of Massachusetts Medical School, Worcester, MA 01605, USA.

\*Corresponding author. Email: pete.demuth@elicio.com

optimize in vivo biodistribution and prevent systemic toxicity of the TLR9 agonist CpG-7909 in the context of severe acute respiratory syndrome coronavirus 2 (SARS-CoV-2) vaccination, while generating strong, long-term cellular and humoral immunity (26, 27). Furthermore, ELI-002, an AMP-CpG adjuvanted peptide vaccine targeting mutant KRAS antigens that drive colorectal and pancreatic cancers, was recently evaluated in a phase 1 clinical trial (AMPLIFY-201; NCT04853017) and an ongoing phase 1/2 trial (AMPLIFY-7P; NCT05726864), showing that AMP-conjugated adjuvants are well tolerated and induce robust antitumor T cell responses associated with tumor biomarker reductions and prolonged relapse-free survival in humans (28, 29).

To build on the potential of this approach, we sought to develop additional adjuvants that use signaling pathways distinct from CpG:TLR9. Viral-like DNA is a promising candidate because of its strong induction of inflammation. The cytosol and endosomes contain numerous nucleic acid-sensing PRRs (30), which can detect a wide range of foreign and host oligonucleotides, generating robust responses by the innate immune system. Nonetheless, to use DNA as a vaccine adjuvant, there are many drug delivery challenges that must be overcome, such as the negligible cellular uptake, rapid clearance, and poor cytosolic access of freely administered DNA (31), which may explain why the development of these DNA-based immunostimulators has been limited thus far. Therefore, targeted delivery of DNA adjuvants to the appropriate innate immune cells in vivo combined with efficient cellular uptake that allows pharmacological activation of cognate PRRs will provide new opportunities with considerable potential to elicit strong immune responses.

In this study, we designed a series of AMP-engineered DNA adjuvants capable of inducing potent CD8<sup>+</sup> and CD4<sup>+</sup> T cell immunity against coadministered protein subunit antigens in mice and NHPs. AMP-induced cellular immune responses substantially exceeded those of comparator vaccines adjuvanted with unmodified “soluble” (SOL) DNA or commercially available adjuvants. Moreover, AMP-mediated production of substantial titers of neutralizing immunoglobulin G1 (IgG1) was accompanied by increased levels of T helper cell 1 (T<sub>H</sub>1)-associated IgG2c, an isotype known to facilitate cellular immunity via antibody-dependent cellular cytotoxicity (ADCC) and complement-dependent cytotoxicity. This was preceded by strong induction of innate responses generating a highly inflammatory, LN-confined milieu resulting in enhanced PRR-sensing, antigen-processing, and antigen-presentation capabilities. These mechanisms were critically reliant on the TANK-binding kinase 1 (TBK1)/IFN- $\beta$  signaling axis as demonstrated by TBK1 deletion and IFN $\alpha$  receptor-1 (IFNAR1) blockade and, to lesser extent, depended on both TLR-mediated as well as RNA-sensing pathways as demonstrated by Unc-93 homolog B1 (Unc93b1) and mitochondrial antiviral-signaling protein (MAVS) deletion. Overall, this study demonstrates the potency of AMP-DNA adjuvants to stimulate robust cellular and humoral immune responses and emphasizes the versatility of AMP modification to efficiently deliver otherwise ineffective adjuvants to potentiate their immunogenicity.

## RESULTS

### AMP-DNA is a potent and safe adjuvant inducing T cell and antibody responses to protein subunit antigens in mice

DNA adjuvants were designed with the objective to stimulate innate immune activation by engaging nucleic acid-sensing PRRs. Multiple

design parameters were assessed, including DNA 5' AMP modification, DNA strandedness, and oligonucleotide sequence, length, and backbone-linkage chemistry. To assess the importance of AMP modification on the immunogenicity of DNA adjuvants, we first synthesized phosphorothioate (PS)-backbone, single- or double-stranded AMP-DNA, consisting of a 5' diacyl phospholipid-conjugated, single-stranded 50-mer polydeoxythymidine ODN alone (AMP-dT<sub>50</sub>) or annealed to a complementary, unconjugated polydeoxyadenosine strand (AMP-dT<sub>50</sub> + dA<sub>50</sub> → AMP-dA:dT<sub>50</sub>; Fig. 1A and fig. S1A). These were compared to their corresponding unmodified SOL DNA analogs. The DNA adjuvants were admixed (Fig. 1B) with either ovalbumin (OVA), a research antigen commonly used to benchmark relative vaccine immunogenicity, or SARS-CoV-2 WH-01-variant spike protein receptor-binding domain (WH-01 RBD), representing a highly relevant antigen of public concern. Subcutaneous immunization demonstrated efficient comigration of vaccine components from the injection site specifically to draining LNs and uptake by APCs (fig. S2). Injections followed a prime-boost regimen with doses on day 0 and day 14 (Fig. 1C). Seven days later, on day 21, cellular immunity was determined via analysis of splenic T cells representing systemic responses secondary to localized priming in the LNs, while analysis of humoral immunity was performed in peripheral blood samples. Immunization with AMP-DNA and OVA resulted in a seven- and 41-fold increase in the mean number of splenic IFN $\gamma$  spot-forming cells (SFCs) for AMP-dA:dT<sub>50</sub> (3962 SFCs/1 × 10<sup>6</sup>) and AMP-dT<sub>50</sub> (6934 SFCs/1 × 10<sup>6</sup>), respectively, compared to their unmodified counterparts, which showed no signal above mock-treated mice (Fig. 1D). Moreover, these responses were polyfunctional, exhibiting significantly increased antigen-specific secretion of IFN $\gamma$  (198-fold), tumor necrosis factor- $\alpha$  (TNF $\alpha$ ; 19-fold), granulocyte-macrophage colony-stimulating factor (GM-CSF; 108-fold), interleukin-2 (IL2; fivefold), and granzyme B (GzmB; 44-fold), when compared to SOL vaccine, which induced responses equivalent to mock treatment (Fig. 1, E and F). Direct tetramer staining of peripheral blood mononuclear cells (PBMCs) without ex vivo stimulation showed that AMP-dA:dT<sub>50</sub> or AMP-dT<sub>50</sub> immunization respectively induced 54 and 70% of circulating CD8<sup>+</sup> T cells to recognize the immunodominant OVA epitope, SIINFEKL (Fig. 1G and fig. S3A). Results from LN-resident immune cells confirmed strong, antigen-specific induction of T cell immunity against SIINFEKL upon immunization with AMP-DNA adjuvants (fig. S1, B and C). Furthermore, intracellular cytokine staining (ICS) of PBMCs demonstrated that CD8<sup>+</sup> and CD4<sup>+</sup> T cells were key contributors of cytokine secretion, with >60% of CD8<sup>+</sup> T cells actively producing IFN $\gamma$  and TNF $\alpha$  (Fig. 1, H and I, and fig. S1D). Similar outcomes were observed in T cells isolated from perfused lung tissue (fig. S1, E and F), an organ that is a frequent point of entry for pathogens and a primary organ for tumor metastasis. No responses were detected in samples of AMP-dT<sub>50</sub> plus OVA-treated animals that were restimulated with dimethyl sulfoxide (DMSO)-vehicle only (fig. S3B) or in mice that had been immunized with AMP-dT<sub>50</sub> in the absence of OVA antigen (Fig. 1G and fig. S3C), demonstrating that the observed immune responses are antigen-specific (gating strategies are depicted in fig. S3, D and E). In addition to strong cellular responses, AMP-modified adjuvants generated high serum IgG titers (Fig. 1J). While SOL groups produced comparable OVA-specific antibody levels, this occurred in the absence of robust cellular immune activation. This may suggest that while humoral responses can be achieved with soluble, unmodified DNA adjuvants, AMP-DNA adjuvants provide specific benefits

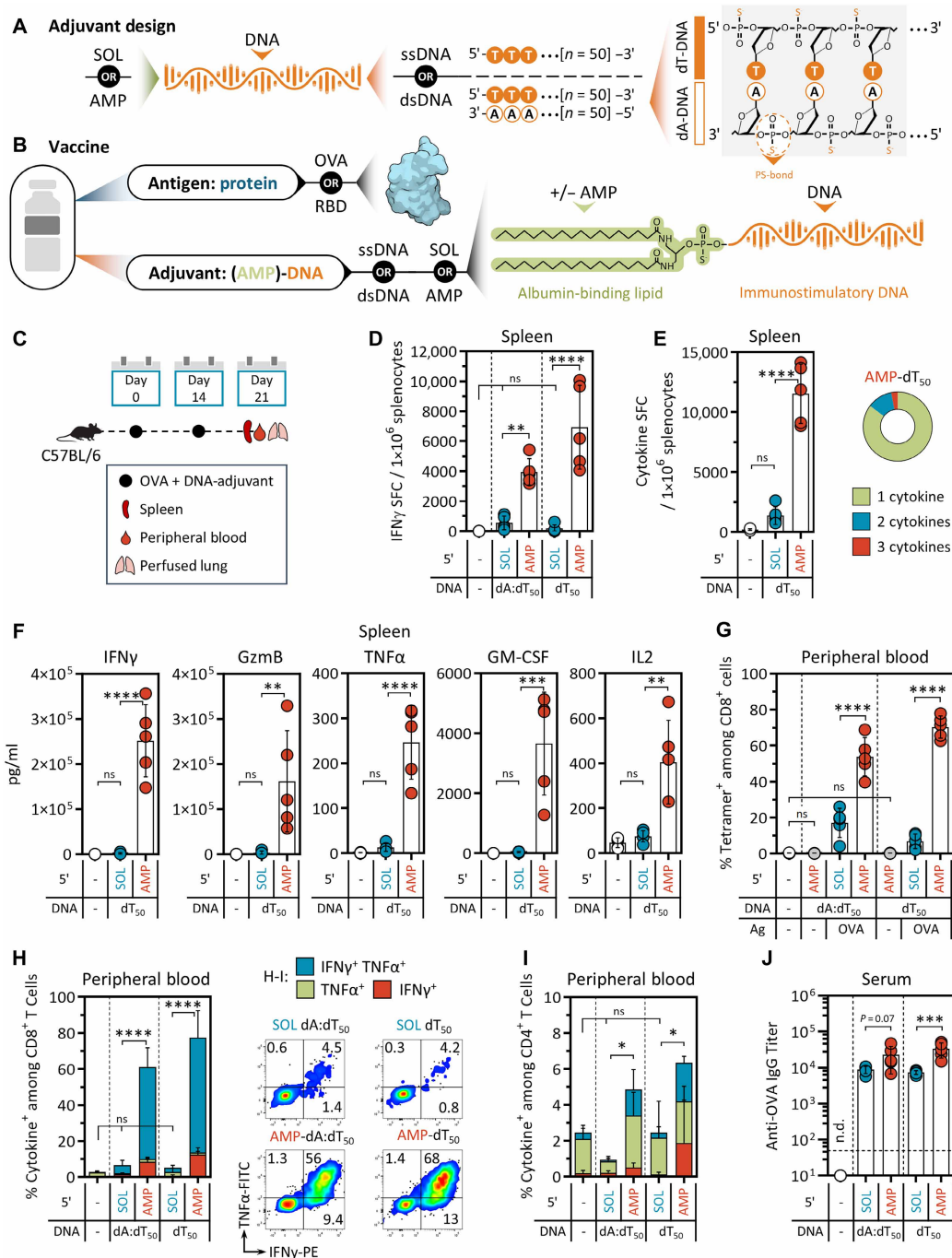


**Fig. 1. AMP-DNA is a potent adjuvant for inducing T cell and antibody responses to protein subunit antigens.** (A) Schematic depicting the chemical structure of AMP-DNA adjuvants. (B) Vaccine formulation consists of the protein antigen (OVA or RBD) admixed with the candidate DNA adjuvants depicted in (A) and fig. S1A, ISD or HSV<sub>60</sub>. (C) Schematic showing animal dosing and experimental schedule. C57BL/6J mice ( $n = 5$ ) were immunized twice with 5  $\mu\text{g}$  of OVA protein and 5 nmol SOL or AMP-DNA adjuvants. AMP adjuvant-only control animals did not receive OVA antigen. Mock vaccines contained vehicle only. Cells were assayed 7 days post-booster dose. (D) ELISpot analysis of splenocytes restimulated with OVA OLPs overnight and assayed for IFN $\gamma$  production. Shown is the frequency of IFN $\gamma$  SFCs per  $10^6$  splenocytes. (E) FluoroSpot analysis of splenocytes restimulated with OVA OLPs overnight and assayed for IFN $\gamma$ , TNF $\alpha$ , and IL2 production. Shown is the frequency of SFCs per  $10^6$  splenocytes that produce at least one cytokine. Donut charts represent percentages of polyfunctional cells. (F) Multiplexed proteomics analysis (Luminex) of splenocytes restimulated with OVA OLPs overnight and assayed for IFN $\gamma$ , GzmB, TNF $\alpha$ , GM-CSF, and IL2 production. Depicted are quantities of secreted cytokines in the culture supernatant. (G) Peripheral blood CD8 $^+$  T cells were assayed ex vivo for OVA reactive TCRs using a SIINFEKL-specific tetramer. (H and I) Flow cytometry analysis of cytokine production by CD8 $^+$  (H) and CD4 $^+$  (I) T cells in peripheral blood. Shown are percentages of cytokine $^+$  cells among CD8 $^+$  or CD4 $^+$  T cells and representative flow cytometry scatter plots of IFN $\gamma$  and TNF $\alpha$  positive CD8 $^+$  T cells. (J) Serum IgG titers were determined against OVA protein. Values depicted are means (SD). \* $P < 0.05$ ; \*\* $P < 0.01$ ; \*\*\* $P < 0.001$ ; \*\*\*\* $P < 0.0001$ , one-way analysis of variance (ANOVA) followed by Tukey's or Šidák's post hoc analysis. dsDNA, double-stranded DNA; n.d., not detected; ns, not significant; ssDNA, single-stranded DNA.

to overcome the more rigorous threshold of activation for robust cellular responses. Analogous results were observed against the RBD antigen (fig. S4). Here, splenic IFN $\gamma$  secretion was enhanced by AMP-dA:dT<sub>50</sub> and AMP-dT<sub>50</sub> over their SOL DNA adjuvant comparators by seven- and 12-fold, respectively (fig. S4B), and resulted in antigen-specific cytokine production in 65 and 85% of circulating CD8<sup>+</sup> T cells (fig. S4D); soluble comparators were inactive. No adverse body weight changes or systemic cytokine levels were observed upon immunization with AMP-DNA, and the primary cytokines implicated in cytokine release syndrome, namely, IL1/2/6/10, IFN $\gamma$ , GM-CSF, and TNF $\alpha$ , were not detected at high levels in the serum (fig. S5). Intramuscular immunization showed comparable immune responses to subcutaneous injections (fig. S6). Together, these data illustrate the potential of AMP-DNA as a potent and safe vaccine adjuvant that can generate strong cellular and humoral immune responses.

### Immunogenicity of AMP-DNA adjuvants depends on key physical and chemical properties

To establish additional physical and chemical characteristics beyond AMP modification that determine optimal immunogenicity of AMP-DNA adjuvants, the remaining four initially selected design parameters (Fig. 2A) were systematically altered to determine their contribution to the resulting immune response. Immunogenicity was determined by measuring antigen-specific IFN $\gamma$  secretion in splenic T cells. Examining DNA strandedness demonstrated that both single-stranded and double-stranded DNA induced robust cytokine production in antigen-specific T cells. While single-stranded AMP-dT<sub>50</sub> generated stronger immune responses than its double-stranded AMP-dA:dT<sub>50</sub> variant (Fig. 2B), two other well-established immunostimulatory ODNs (32), herpes simplex virus 60 (HSV<sub>60</sub>) and *Listeria monocytogenes*-derived IFN-stimulatory DNA (ISD), performed equally well in either configuration upon AMP conjugation. Therefore, strandedness may not be a crucial characteristic for adjuvant recognition depending on the DNA sequence (Fig. 2, C and D). These results also suggest that cellular DNA sensing may be largely sequence-agnostic as significant responses were observed to all aforementioned sequences. In contrast, single-stranded polydeoxyadenosine (AMP-dA<sub>50</sub>) as well as AMP-dT:dA<sub>50</sub>, which contains the AMP modification on the dA strand, were unable to generate robust immunity (Fig. 2B). However, an ODN composed of alternating deoxythymidine and deoxyadenosine bases (dAdT:dAdT<sub>50</sub>) was able to substantially rescue immune responses (fig. S7), suggesting that certain sequence requirements do exist and that deoxythymidine containing sequences may be preferred by the relevant DNA-sensing PRRs. Another crucial factor known to determine DNA detection by PRRs is ODN length (32). Systematic variation of sequence length for AMP- and SOL DNA showed that sequences shorter than 30 nucleotides were unable to generate T cell responses (Fig. 2, E and F), indicating that the involved PRRs require a minimum sequence length to transmit the danger signal. However, increasing DNA length beyond 30 to 50 nucleotides did not confer additional benefits. Last, exchanging the synthetic PS bonds with naturally occurring phosphodiester (PO) bonds abrogated all cellular immune responses (Fig. 2, G and H), possibly due to poor *in vivo* stability of PO bonds due to nuclease-dependent degradation. Overall, these data suggest that the optimal single- or double-stranded AMP-DNA adjuvant should contain 30 to 50 PS-linked nucleotides, of which a sufficient number are deoxythymidine for effective PRR recognition.

To further elucidate the importance of adjuvant design on immunogenicity, *in vivo* imaging was conducted in which DNA was 3'-conjugated to a Cy5 fluorescent tag to allow analysis of adjuvant biodistribution upon injection. dT variants of 50 and 20 nucleotides in length were selected, representing examples with potent immunogenic activity or complete lack thereof, respectively. As expected, given their hydrodynamic size (>10 nm), both SOL and AMP-dT<sub>50</sub> efficiently accumulated in the inguinal LNs (13), whereas the shorter SOL dT<sub>20</sub> failed to do so (fig. S8, A to C). AMP modification, however, was able to reinstate efficient delivery of AMP-dT<sub>20</sub>, consistent with prior observations for similarly sized CpG-7909 (23). This suggests that DNA molecules of small size are poor adjuvants partly due to their untargeted systemic distribution, with only small quantities reaching immunologically relevant cells within the LNs. In addition, immune activation requires sufficient DNA length, as even when AMP-dT<sub>20</sub> efficiently reaches the LN, it is incapable of stimulating an immune response (Fig. 2E). Notably, SOL dT<sub>50</sub> as well as SOL dA:dT<sub>50</sub> (fig. S8, D and E) were incapable of eliciting responses despite reaching the LNs and being of sufficient length. Therefore, AMP modification may facilitate additional mechanisms beyond LN delivery, which are critical for immune activation: Improved cellular uptake by APCs, endocytic escape leading to enhanced cytosolic PRR access, or other mechanisms promoting cognate PRR engagement are possible factors of great interest for future studies.

### AMP-DNA adjuvants generate highly durable memory responses with significant recall potential

To further determine whether these robust acute responses translated into durable immune memory, longitudinal studies following animals for up to 9 months after prime-boost immunization with AMP-DNA and RBD antigen were conducted. AMP-dT<sub>50</sub>-immunized mice showed a stable population of RBD-specific peripheral blood T cells for the entire duration of the study, plateauing at >31% of CD8<sup>+</sup> T cells that produced cytokines upon RBD-peptide stimulation (Fig. 3A) and >12% that expressed T cell receptors (TCRs) specific to the VNFNFNGL epitope of RBD (Fig. 3B). Over 239 days, RBD-specific CD8<sup>+</sup> T cells transitioned from mostly effector and/or effector memory phenotype (CD44<sup>+</sup>/CD62L<sup>-</sup>) to predominantly (62%) central memory phenotype (CD44<sup>+</sup>/CD62L<sup>+</sup>; Fig. 3C). Upon recall exposure to antigen on day 244, these readily converted back into effector and/or effector memory T cells. This recall response rebounded the population of RBD-specific, cytokine-secreting effector T cells to 55% of circulating CD8<sup>+</sup> T cells and expanded VNFNFNGL-specific T cells to 35% (Fig. 3, A and B). Effector T cell expansion was also observed among splenocytes, where the number of cytokine-producing cells doubled in response to RBD antigen (21,300 SFCs/10<sup>6</sup> splenocytes) compared to unchallenged littermates (10,700 SFCs/10<sup>6</sup>; Fig. 3D). As central memory cells generally home to secondary lymphoid tissues, we examined the enrichment of such memory cells in LNs. Nine months after mice were immunized with AMP-dT<sub>50</sub>, 5.8% of all LN-resident CD8<sup>+</sup> T cells were RBD-specific central memory cells, providing a significant pool of cells poised to remobilize in the event of antigen encounter (Fig. 3E). Identical trends were observed in AMP-dA:dT<sub>50</sub>-treated mice (fig. S9, A to D). Despite these potent and prolonged responses, the effector and/or effector memory cells did not exhibit any signs of exhaustion (fig. S9E). As CD4<sup>+</sup> T cells facilitate cellular and humoral responses, their activation status was also investigated. These cells followed a similar trend to CD8<sup>+</sup> T cells, establishing a plateau of significant

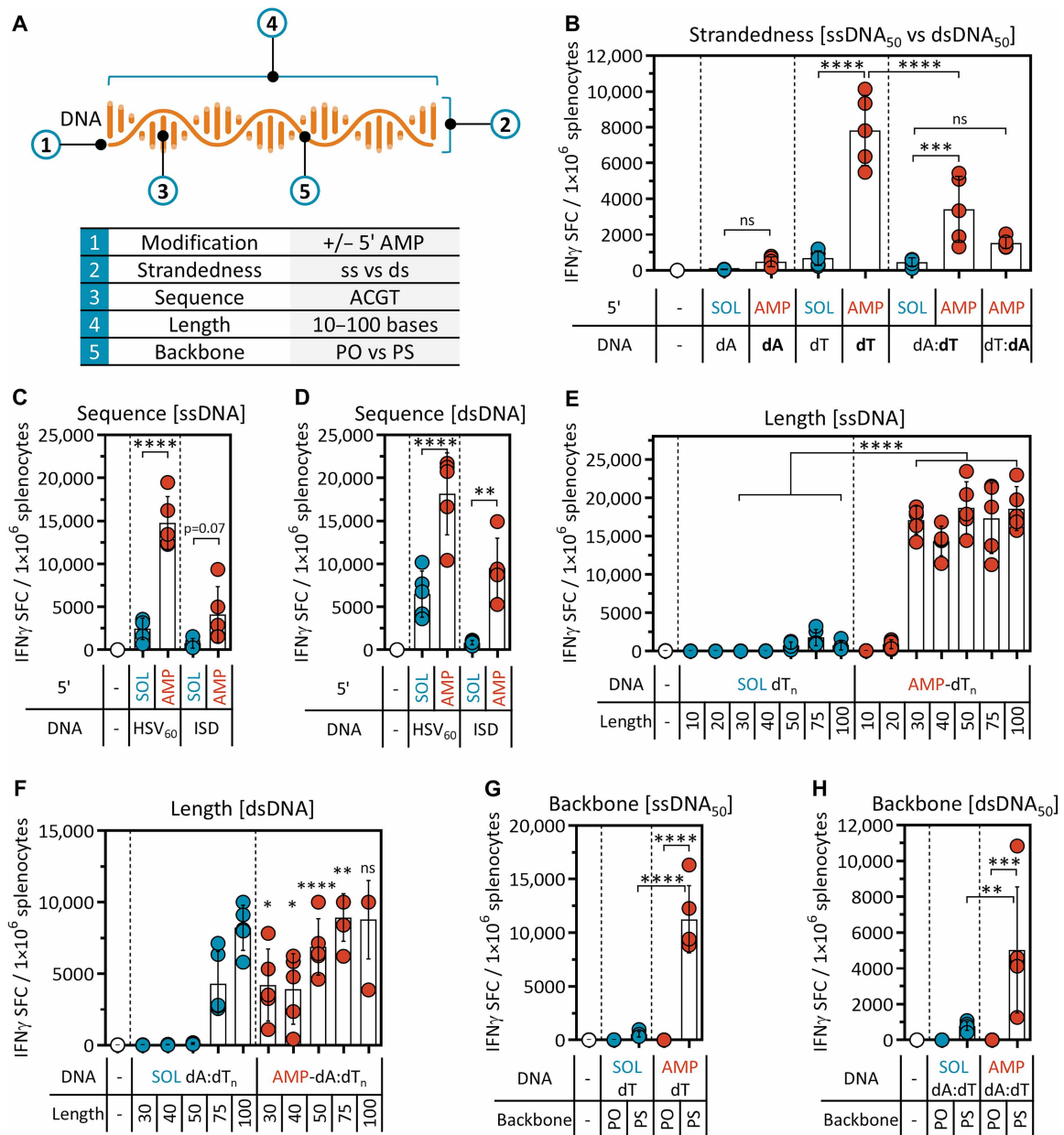


**Fig. 2. DNA design features dictate the strength of resulting immunogenicity.** C57BL/6J mice ( $n = 5$ ) were immunized as described in Fig. 1C. Immunizations contained 5  $\mu$ g of WH-01 RBD protein and 5 nmol SOL or AMP-DNA adjuvant. Cells were assayed 7 days post-booster dose. (A) Schematic describing the modifications of the DNA adjuvants. (B to H) Evaluation of the effect of DNA modifications on immune activation. Splenocytes were restimulated with RBD OLPs overnight and assayed for IFN $\gamma$  production by ELISpot. Shown is the frequency of IFN $\gamma$  SFCs per  $10^6$  splenocytes; The assessed DNA modifications included (B) single-stranded versus double-stranded DNA (bold letters indicate the AMP-conjugated strand); [(C) and (D)] HSV<sub>60</sub> and ISD sequences in single-stranded (C) and double-stranded (D) form; [(E) and (F)] DNA length variants for dT (E) and dA:dT (F); and [(G) and (H)] PO- versus PS-linked bases for dT (G) and dA:dT (H). Mock vaccines contained vehicle only. Values depicted are means (SD). \* $P < 0.05$ ; \*\* $P < 0.01$ ; \*\*\* $P < 0.001$ ; \*\*\*\* $P < 0.0001$ , one-way ANOVA followed by Tukey's or Šidák's post hoc analysis. Statistical analyses in (E) and (F) compare each AMP-modified length variant to its soluble counterpart.

magnitude during the memory response phase compared to SOL DNA-treated animals. Upon antigen recall, CD4<sup>+</sup> T cell levels exceeded those observed during the acute phase (fig. S9, F and G). These cellular long-term responses against RBD were substantiated in a model using OVA (fig. S9, H and I). Furthermore, longitudinal analysis of anti-OVA antibody titers in these mice demonstrated trends analogous to those observed with cellular responses. IgG antibody levels were maintained at high concentrations throughout

the study, rebounded significantly after antigen challenge on day 218, and were comparable with those seen in animals treated with Alhydrogel [aluminum hydroxide gel (alum)], an adjuvant known for its induction of strong humoral responses (fig. S10). Overall, these data indicate that AMP-DNA adjuvants have the potential to generate long-lasting cellular and humoral memory responses that can quickly expand upon detection of subsequent antigen exposure.

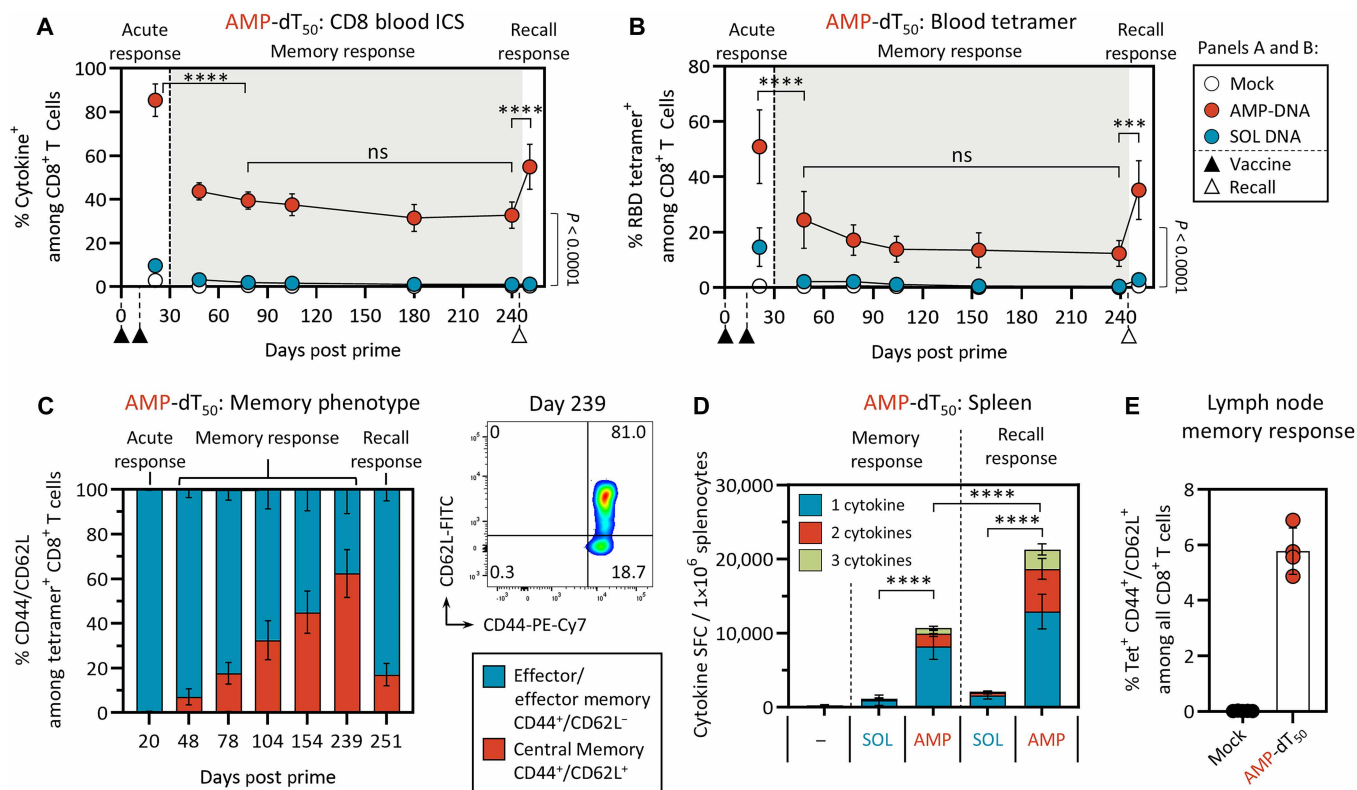


**Fig. 3. AMP-DNA adjuvants elicit highly durable T cell responses with significant recall potential 8 months postvaccination.** C57BL/6J mice ( $n = 10$ ) were immunized twice (black triangles) with 5  $\mu\text{g}$  of WH-01 RBD and either 5 nmol SOL or AMP-dT<sub>50</sub> adjuvant. Mock vaccines contained vehicle only. White triangles indicate antigen challenge with RBD protein alone. (A to C) Peripheral blood samples were collected longitudinally over 8 months and analyzed via flow cytometry. (A) IFN $\gamma$  and TNF $\alpha$  secreting CD8<sup>+</sup> T cells reactive to overnight stimulation with RBD OLPs. (B) CD8<sup>+</sup> T cells with TCRs specific to VNFNFGFL-tetramer. (C) Effector/effector memory phenotype marker expression (CD44 and CD62L) on RBD-tetramer specific CD8<sup>+</sup> cells from AMP-DNA immunized mice (left) and representative scatter plot on day 239 post-prime immunization (right). (D) FluoroSpot analysis of cytokine secreting splenocytes upon overnight stimulation with RBD OLPs and assayed for IFN $\gamma$ , TNF $\alpha$ , and IL2 production. “Recall response” mice ( $n = 5$ ) were antigen challenged on day 244 and analyzed 7 days later, on day 251, whereas “memory response” mice ( $n = 5$ ) remained unchallenged. (E) Percentage of RBD-specific central memory T cells in LNs of AMP-dT<sub>50</sub>-immunized mice 9 months after primer dose (day 272). Shown are percentages of CD8<sup>+</sup> T cells that are triple-positive for RBD tetramer, CD44, and CD62L among all LN-resident CD8<sup>+</sup> T cells. Gray-shaded areas in (A) and (B) represent memory response, whereas adjacent unshaded areas represent the acute and recall responses. Statistics in (A) and (B) compare the longitudinal changes in immune response within the AMP-DNA-treated groups.  $P$  value on the right side of the graph represents the time point with least significant difference between AMP and SOL DNA-treated cohorts. Values depicted are means (SD). \*\*\* $P < 0.001$ ; \*\*\*\* $P < 0.0001$ , one-way ANOVA followed by Tukey’s post hoc analysis.

### AMP-DNA induces superior cellular and strong humoral immunogenicity relative to clinical benchmark adjuvants

To test how AMP-DNA adjuvants compare to commercially available and/or clinically used adjuvants, we selected a panel that included examples of common vaccine adjuvants available for use in humans. These benchmark comparators included alum; a group of oil-and-water emulsions including incomplete Freund’s adjuvant (IFA), Ad-aVax (an MF59 mimetic), and AddaS03 (an AS03 mimetic); the TLR4 agonist monophosphoryl lipid A (MPLA; a lipopolysaccharide derivative); and poly(I:C) (4, 33). AMP-CpG-7909 was also included in this panel to compare among AMP-conjugated adjuvants. AMP-DNA consistently produced significantly higher cellular responses than any of the benchmark adjuvants or even AMP-CpG-7909. Both AMP-dT<sub>50</sub> and AMP-dA:dT<sub>50</sub> generated greater numbers of circulating antigen-specific CD8<sup>+</sup> T cells (Fig. 4A) and increased frequencies of cytokine<sup>+</sup> CD8<sup>+</sup> and CD4<sup>+</sup> T cells in peripheral blood, splenic, and perfused lung samples (Fig. 4, B to F, and fig. S11), whereas benchmark comparators did not elicit any notable cellular immunity. In contrast, all adjuvants were able to generate high titers

of anti-OVA serum IgG (Fig. 4G). However, more detailed analysis of specific IgG subclasses, namely, IgG1 and IgG2c [an IgG2a paralog in C57BL/6 mice; (34)], showed differences in isotype profiles. While titers of IgG1, whose main function is to neutralize soluble antigens, were comparable in all adjuvant groups tested, AMP-DNA and AMP-CpG vaccines generated one to two orders of magnitude higher levels of IgG2c, an IFN $\gamma$ -induced isotype that strongly promotes complement-fixing and ADCC (Fig. 4, H to J) (35). This is consistent with the significant levels of IFN $\gamma$  produced by effector T cells in these mice. This demonstrates that AMP-conjugated DNA adjuvants were capable of complementing robust humoral with strong cellular immune activation.

### In NHP, AMP-dT<sub>50</sub> induces cross-protective cellular and humoral immune responses to multiple RBD variants of concern

Encouraged by the immune responses elicited by AMP-DNA in mice, AMP-dT<sub>50</sub> was assessed in rhesus macaque NHPs for activity predictive of potential responses in humans using a relevant

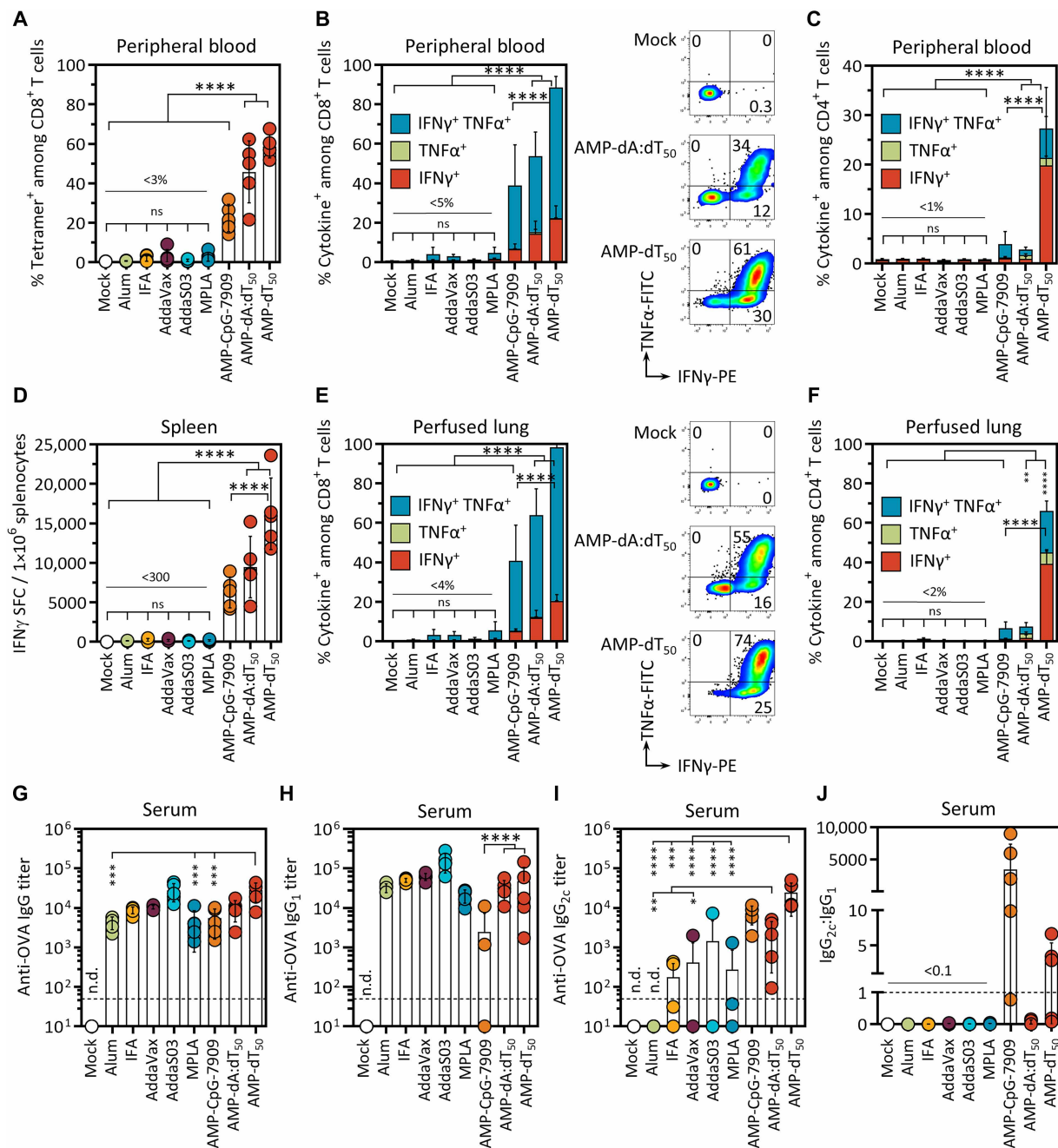


**Fig. 4. AMP-DNA induces superior cellular and strong humoral immunogenicity relative to clinical benchmark adjuvants.** C57BL/6J mice ( $n = 5$ ) were immunized as described in Fig. 1C. Immunizations contained 5  $\mu$ g of OVA protein and either 5 nmol AMP-DNA, 1 nmol AMP-CpG-7909, or the indicated comparator adjuvants (100  $\mu$ g of alum; 10  $\mu$ g of MPLA; 1:2 emulsions of IFA, AddaVax, and AddaS03). Cells were assayed 7 days post-booster dose. **(A)** Peripheral blood CD8<sup>+</sup> T cells were assayed ex vivo for OVA-reactive TCRs using a SIINFELK-specific tetramer. **(B and C)** Flow cytometry analysis of cytokine production by CD8<sup>+</sup> (B) and CD4<sup>+</sup> T cells (C) in peripheral blood. Shown are percentages of cytokine<sup>+</sup> cells among CD8<sup>+</sup> or CD4<sup>+</sup> T cells and representative flow cytometry dot plots of TNF $\alpha$  and IFN $\gamma$  positive CD8<sup>+</sup> T cells. **(D)** ELISpot analysis of splenocytes restimulated with OVA OLPs overnight. Shown is the frequency of IFN $\gamma$  SFCs per 10<sup>6</sup> splenocytes. **(E and F)** Flow cytometry analysis of cytokine production by CD8<sup>+</sup> (E) and CD4<sup>+</sup> T cells (F) in perfused lung tissue. Representation same as (B) and (C). **(G to I)** Serum anti-OVA pan-IgG (G), IgG1 (H), and IgG2c (I) titers were determined against OVA protein. **(J)** Ratio of IgG2c:IgG1 antibody response from (H) and (I). Mock vaccines contained antigen only. Values depicted are means (SD). In panels where multiple groups are statistically compared to each other, both AMP-dT<sub>50</sub> and AMP-dA:dT<sub>50</sub> are significantly different to all other indicated groups as shown. \* $P < 0.05$ ; \*\* $P < 0.01$ ; \*\*\* $P < 0.001$ ; \*\*\*\* $P < 0.0001$ , one-way ANOVA followed by Tukey's post hoc analysis.

SARS-CoV-2 model. Three adult, female macaques were immunized subcutaneously in each upper thigh with WH-01 RBD protein admixed with AMP-dT<sub>50</sub> at week 0 (baseline) and week 4; PBMC, serum, and LN fine-needle aspirates (FNAs) were collected for analysis of cellular and humoral immunity as illustrated in Fig. 5A. At week 6, 2 weeks after the booster dose, significant increases in the frequency of IFN $\gamma$  SFC were observed among peripheral blood T cells upon stimulation with WH-01 RBD overlapping peptides (OLPs) compared to prevaccination baseline values in all three animals (Fig. 5B). Moreover, CD4<sup>+</sup> T cells exhibited significantly increased production of IFN $\gamma$ , TNF $\alpha$ , and IL2 cytokines, and responses in CD8<sup>+</sup> T cells were elevated compared to baseline (Fig. 5, C and D). Similar cellular responses were observed when PBMCs from WH-01-immunized animals were stimulated with OLPs to SARS-CoV-2 variants of concern (VOCs), Beta and Delta RBD (fig. S12, A to C), suggesting that AMP-dT<sub>50</sub> is able to generate robust cellular responses to

conserved epitopes potentially important for protection across different strains of SARS-CoV-2. To investigate the humoral response, serum samples were collected in 2-week intervals starting at pre-treatment baseline (Fig. 5E). WH-01 RBD-specific IgG levels were assessed by enzyme-linked immunosorbent assay (ELISA) and converted into World Health Organization (WHO) binding antibody units (BAU) per milliliter. All three animals achieved seroconversion with significantly increased anti-RBD-specific IgG concentrations after only one immunization and reached peak levels 2 weeks after the second dose. Elevated antibody titers were maintained throughout the assessed study period. When examining antibody responses to Beta, Delta, and Omicron RBD variants, the same trends were observed (fig. S12, D and E), substantiating the notion that AMP-dT<sub>50</sub> adjuvants may generate cross-protective immunity to multiple VOC. To ascertain whether these antibody responses were able to provide neutralizing immunity, which protects against SARS-CoV-2 before

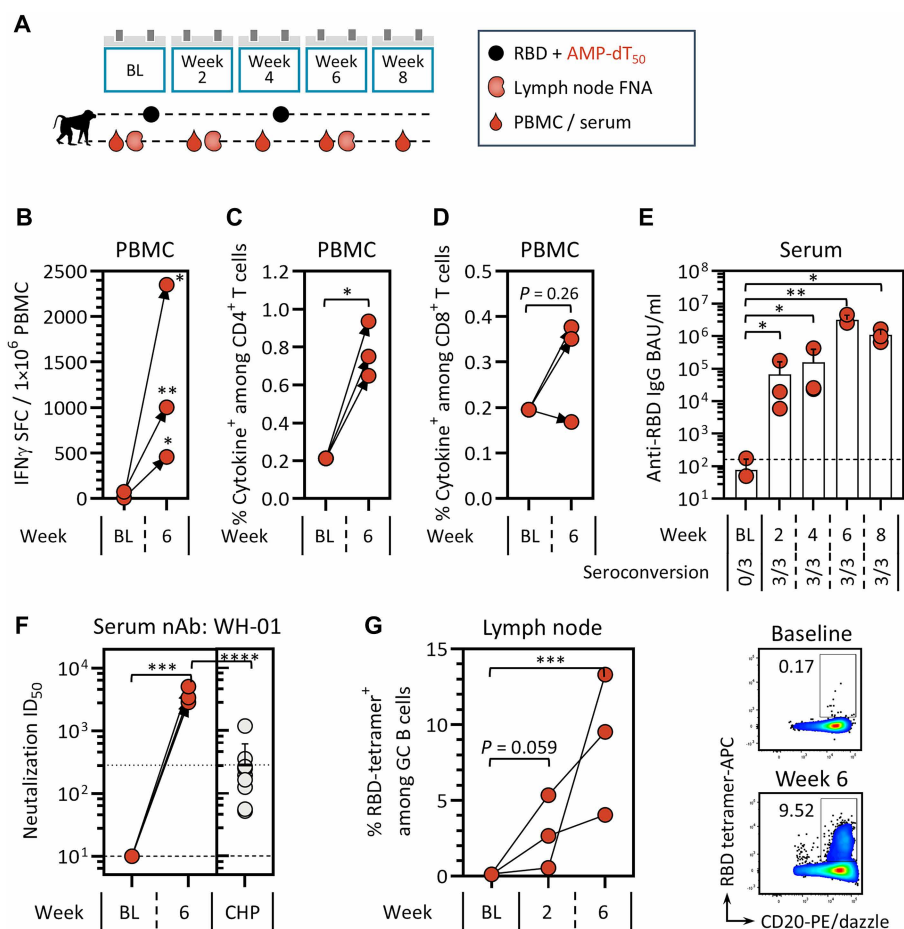


**Fig. 5. AMP-dT induces potent cellular and humoral immunity in NHPs.** Cellular and humoral responses to WH-01 RBD and AMP-DNA adjuvant were assessed in rhesus macaques. (A) Three animals were immunized at week 0 (baseline, BL) and four with 140  $\mu$ g of WH-01 RBD protein admixed with 5 mg of AMP-dT<sub>50</sub>. (B to D) PBMCs were collected at baseline and week 6 and stimulated with WH-01 RBD OLPs overnight. (B) IFN $\gamma$  ELISpot analysis. Shown are IFN $\gamma$  SFCs per  $1 \times 10^6$  PBMCs. [(C) and (D)] Flow cytometry analysis of cytokine production by CD4<sup>+</sup> and CD8<sup>+</sup> T cells. Shown are frequencies of combined IFN $\gamma$ , TNF $\alpha$ , and IL2 cytokine production. (E) For antibody response assessment, serum was collected at baseline and weeks 2, 4, 6, and 8. RBD-specific serum IgG BAU were assessed for WH-01 at each time point. (F) For neutralizing antibody (nAb) response assessment through pseudovirus inhibition serum was collected at baseline and week 6. Shown are ID<sub>50</sub> values for WH-01 in comparison to CHP. The dashed lines in (E) and (F) represent the lower limit of detection discriminating between samples positive or negative for seroconversion. The dotted line in (F) represents the mean value observed for the human plasma comparators. (G) For GC B cell assessment LN FNAs were collected at baseline and weeks 2 and 6. Shown are frequencies of RBD-specific GC B cells (CD20<sup>+</sup> Bcl6<sup>+</sup> Ki-67<sup>+</sup>) in individual animals over time with corresponding representative flow cytometry scatter plots of RBD-specific B cells. Values depicted are means (SD). \* $P < 0.05$ ; \*\* $P < 0.01$ ; \*\*\* $P < 0.001$ ; \*\*\*\* $P < 0.0001$ , paired t test.

infection occurs, pseudovirus inhibitory activity was assessed (Fig. 5F and fig. S12, F and G). The antibody response in all animals provided neutralizing protection against the tested VOC at significantly greater median infective dose (ID<sub>50</sub>) values than convalescent human plasma (CHP) from patients who had recently recovered from SARS-CoV-2 infection, suggesting that AMP-dT<sub>50</sub>-induced immunity may exceed response levels generated by natural infection in humans. This humoral response directly correlated with robust germinal center (GC) formation in these animals as determined by flow cytometry analysis of GC B cell (CD20<sup>+</sup> Bcl6<sup>+</sup> Ki-67<sup>+</sup>) specificity to the RBD antigen in LN FNA (Fig. 5G), a prerequisite to affinity maturation and generation of highly specific antibodies. The immunogenicity of this AMP-dT<sub>50</sub> adjuvanted SARS-CoV-2 vaccine was not accompanied by overt adverse effects observable by clinical evaluation (body temperature, weight, and injection site observations; fig. S13, A and B). Serum cytokine levels (fig. S13C) and complete blood cell counts (fig. S13, D to H) transiently fluctuated (IFN $\gamma$ , IL-1RA, and IL18) upon administration of AMP-dT<sub>50</sub> but normalized after 1 to 2 days. The increase in IL18 levels may suggest an involvement of the inflammasome in NHPs, whereas in mice, this pathway was shown to not play a role. Together, the strong cellular and humoral responses and minimal adverse effects observed in NHP, combined with clinical data using a similar AMP-conjugated CpG adjuvant (28), indicate promise for AMP-DNA adjuvant evaluation in future clinical studies.

### AMP-DNA promotes a highly immunostimulatory milieu in LNs of mice and NHP

The improved immunogenicity of AMP adjuvants has been correlated with their enhanced delivery to draining LNs (23, 24). To elucidate the mechanisms within LNs that facilitate AMP-DNA-induced immunity, a comprehensive panel of >500 immune-relevant gene transcripts was evaluated in mice and NHP using NanoString. Mice were immunized once with WH-01 RBD antigen and dT<sub>50</sub> DNA; subsequently, inguinal LNs were collected for transcriptome assessment at the indicated times (Fig. 6A). After 6 hours, mice treated with AMP-dT<sub>50</sub> displayed an acute up-regulation of dozens of transcripts essential to mounting an effective innate immune response (fig. S14, A to C). Up-regulated genes included chemokines associated with APC recruitment to the LNs, APC lineage and activation markers, PRRs, and transcripts that facilitate antigen processing and presentation, consistent with professional APC influx and subsequent robust innate immunity. In contrast, mice treated with SOL dT<sub>50</sub> displayed a much more restricted transcriptional signature limited to a few chemokines. Twenty-four hours after AMP-dT<sub>50</sub> immunization, the initial innate immune response developed into a fully matured proinflammatory milieu, characterized by multiple axes of immune pathway activation critical to adaptive immunity, while SOL dT<sub>50</sub> failed to do so (Fig. 6, B to D, and fig. S14D). Of particular interest were gene profiles indicating enhanced immune functions of activated APCs to recognize danger signals {e.g., *Tbk1*, *Ddx58* [retinoic acid-inducible gene I (RIG-I)], *Ifih1* [melanoma differentiation-associated protein 5 (MDA5)], *Tlr3*, *Tlr9*, and *MyD88*}, to process and present antigens (e.g., *H2-k1*, *Tap1*, *B2m*, *Psmb9/10*, *Ctss*, and *Ctsc*), to costimulate T cells (e.g., *Cd80*, *Cd86*, and *Cd40*), to signal via cytokines (e.g., *Tnfa*, *Il18*, *Stat2/3*, and *Jak2*), and to induce numerous antiviral interferon-stimulated genes (ISGs) such as from the *Irf*, *Ifi*, and *Ddx* family of genes, among many others. At 72 hours

postadministration of AMP-dT<sub>50</sub>, this inflammatory response had subsided, with PRRs as well as cytokine and chemokine levels returning to baseline (fig. S14, E to G). Nonetheless, a large contingent of cells expressing CD11b (*Itgam*) transcripts remained in the LN. At these early time points, no elevation of transcripts associated with increased overall T cell populations was observed relative to untreated groups. Of note, the transcriptome of SOL dT<sub>50</sub>-treated LNs started to develop B cell-associated signatures (*Cd19/22/79a/81*, *Btk*, and *Pax5*) at the 72-hour time point (fig. S14E), corresponding with the predominantly humoral response observed in these animals (Fig. 1H).

Similar results were observed in NHPs upon immunization with WH-01 RBD admixed with AMP-dT<sub>50</sub>. Transcriptome analysis of collected LNs showed the up-regulation of multiple chemokines and cell adhesion molecules 24 hours after AMP-dT administration compared to prevaccination baseline values, suggesting an influx of innate immune cells (fig. S15, A and B). At 48 hours, this was followed by further augmentation of a wide range of proinflammatory pathways (Fig. 6, E and F, and fig. S15, C and D). The increased transcriptional signature of various APCs in the LN including dendritic cells (DCs) and macrophages [*Fcgr3* (CD16), *Fcgr2a/b* (CD32), *Fcgr1a* (CD64), *Itgam* (CD11b), and *Itgax* (CD11c)] correlated with a highly antiviral environment (*Oas1/2/3*, *Ifit1/2/3*, and *Irf5/7*) sensitive to nucleotide detection [*Ddx58* (RIG-I), *Ddx60*, *Ifih1* (MDA5), *Mb21d1* (cGas), and *OasL*]. These transcriptional features were consistent with the development of an inflammatory niche supportive of the adaptive immune responses observed with AMP-DNA immunizations in NHP (Fig. 5). Across mice and NHPs, AMP-dT<sub>50</sub> activated numerous shared immune pathways required to convert the naïve LN into a proinflammatory hotspot (fig. S15E). Correlation of these transcriptional patterns to immunogenicity further highlights the importance of engaging the innate immune system in this specialized organ, which is an optimal environment for robust immune activation.

### AMP-DNA potently induces inflammatory cytokine responses dependent on IFN-I signaling

Given the notable induction of immunostimulatory transcriptional programs upon vaccination with AMP-DNA, we investigated whether these effectively translated into changes in the proteomic profile within the LNs. Mice were immunized with one dose of WH-01 RBD and AMP-dT<sub>50</sub> or AMP-dA:dT<sub>50</sub> or their respective soluble counterparts, and draining LNs were collected 6 or 24 hours later for multiplexed proteomic analysis. AMP-dT<sub>50</sub>-treated animals (Fig. 7A and fig. S16) exhibited a significant boost in the production of nearly all tested cytokines over mock- or SOL dT<sub>50</sub>-treated mice at the 24-hour time point, consistent with mRNA transcript levels at that time. These cytokines included (i) growth factors (granulocyte colony-stimulating factor, GM-CSF, and macrophage colony-stimulating factor), (ii) proinflammatory cytokines (IFN $\gamma$ , TNF $\alpha$ , and IL6), (iii) chemokines [interferon-gamma induced protein 10 kDa (IP-10), IL8, monocyte chemoattractant protein-1 (MCP1), macrophage inflammatory protein-1 (MIP1 $\alpha/\beta$ ), and monokine induced by gamma interferon (MIG)], (iv) inflammasome-associated cytokines (IL1 $\beta$  and IL18), and (v) IFN-I, consistent with the ISG signature observed above. Similarly, mice immunized with AMP-dA:dT<sub>50</sub> (fig. S17) had high levels of cytokine production at 24 hours but appeared to initiate production earlier than the single-stranded form. In contrast, cytokine levels in SOL dA:dT<sub>50</sub>-treated LNs were significantly lower

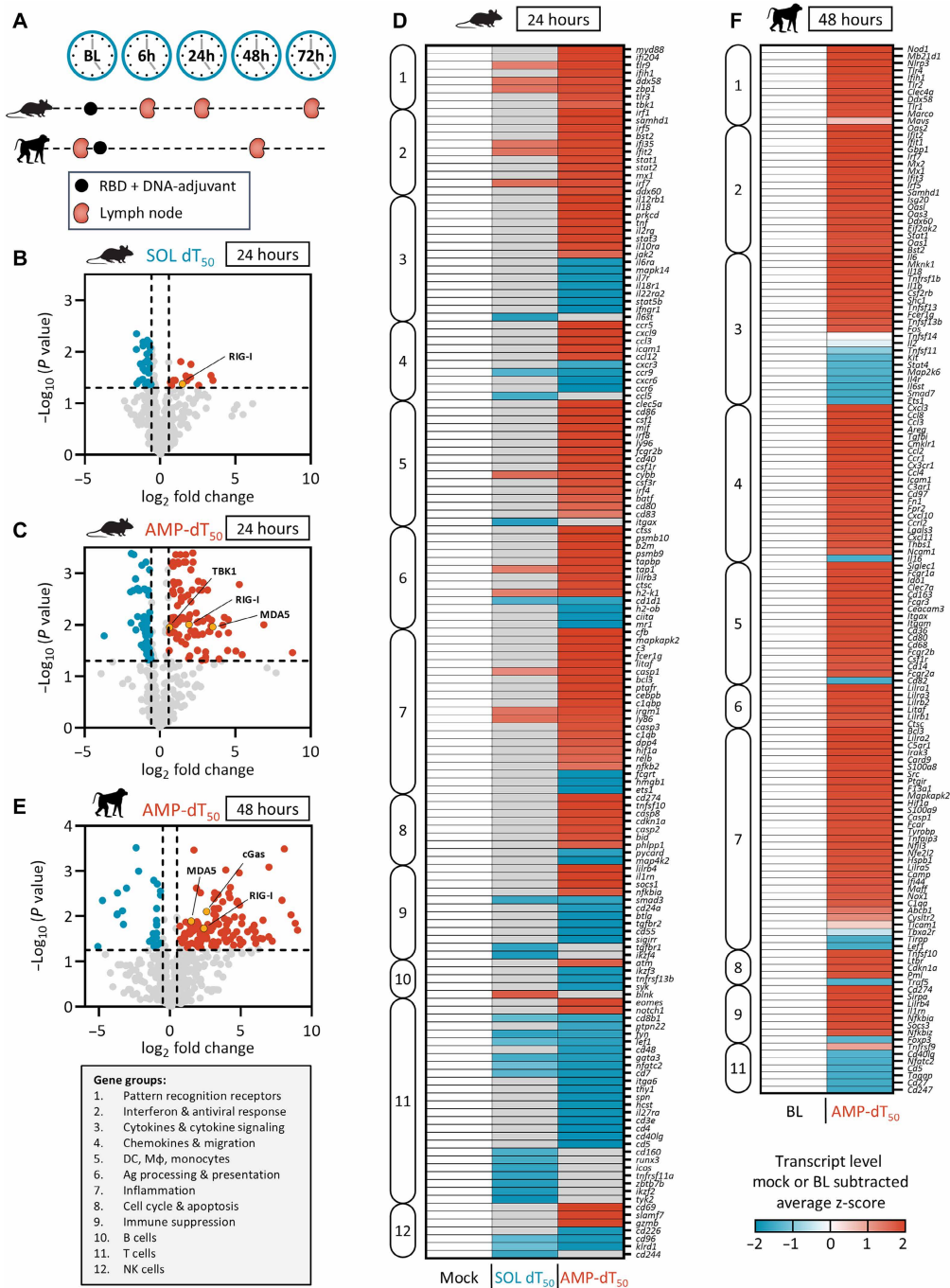


**Fig. 6. AMP-DNA promotes comprehensive inflammatory transcriptional reprogramming in draining LNs of mice and NHP.** (A) Schema showing animal dosing and experimental schedule. C57BL/6J mice ( $n = 2$ ) were immunized once with  $5 \mu\text{g}$  of WH-01 RBD protein admixed with  $5 \text{ nmol}$  SOL or AMP-dT<sub>50</sub> adjuvants. Whole LN lysates were assayed by NanoString nCounter Mouse Immunology Panel at the indicated time points post-primer dose. Rhesus macaques ( $n = 2$ ) were immunized once with  $140 \mu\text{g}$  of WH-01 RBD protein admixed with  $5 \text{ mg}$  of AMP-dT<sub>50</sub> adjuvant. LN FNAs were collected prior to week 10 booster (baseline) and 48 hours after booster immunization and analyzed by NanoString nCounter NHP Immunology Panel. (B and C) Volcano plot representation of log-transformed transcript values from SOL dT<sub>50</sub> (B) and AMP-dT<sub>50</sub> (C) immunized mice at 24 hours (red values are significantly up-regulated and blue values are significantly down-regulated gene transcripts that changed by a minimum of 1.5-fold). Dashed horizontal line represents significance threshold ( $P = 0.05$ ); vertical dashed lines represent fold-change limits of  $\pm 1.5$ . (D) Heatmap representation of transcript expression 24 hours after immunization. Shown are mock-subtracted, average z-scores of transcripts that are significantly changed in at least one treatment group and that are either  $\geq 1.5$ -fold up-regulated (red) or down-regulated (blue) compared to mock treatment. Mock vaccines contained PBS vehicle only. Insignificant values ( $P \geq 0.05$ ) are shown in gray. (E) Volcano plot representation of log-transformed transcript values from AMP-dT<sub>50</sub> immunized NHP at 48 hours after immunization [significance and fold-change thresholds as in (B) and (C)]. (F) Heatmap representation of LN FNA mRNA analyzed 48 hours after immunization. Shown are baseline-subtracted, average z-scores of transcripts that are significantly changed and are either  $\geq 1.5$ -fold up-regulated (red) or down-regulated (blue) compared to baseline. Genes were clustered into 12 groups (box insert) using Gene Ontology and UniProt databases. h, hours; NK cells, natural killer cells.

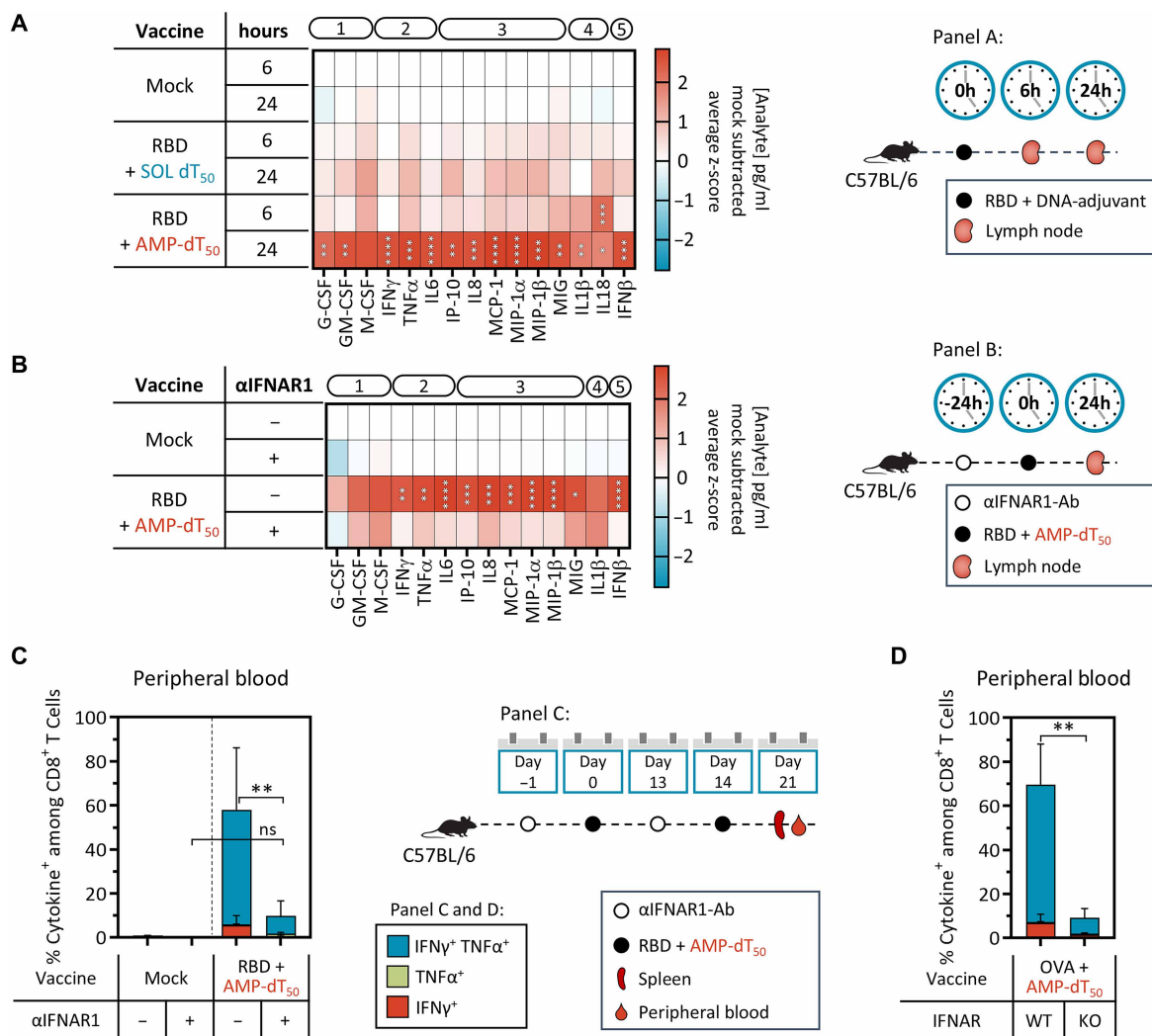


**Fig. 7. AMP-dT<sub>50</sub> potently induces an inflammatory proteomic milieu in draining LNs that is dependent on IFN-I signaling.** (A) C57BL/6J mice ( $n = 5$ ) were immunized once with 5  $\mu$ g of WH-01 RBD protein and 5 nmol SOL or AMP-conjugated dT<sub>50</sub>. LNs were collected and processed for protein extraction and analysis by Luminex at 6 and 24 hours postimmunization. Analyte concentrations were expressed in a heatmap showing mock-subtracted z-scores of analyte concentrations (pg/ml). Analytes are annotated by functional category: (i) growth factors, (ii) inflammatory cytokines, (iii) chemokines, (iv) inflammasome, and (v) IFN-I. Statistical analysis compares AMP-DNA-treated groups with time point-matched SOL DNA groups. (B) C57BL/6J mice ( $n = 5$ ) were dosed intraperitoneally with IFNAR1 blocking antibody or isotype control 24 hours prior to immunization as in (A). Protein from LNs was extracted 24 hours postimmunization. Heatmap representation and analyte annotation as in (A). Statistical analysis compares IFNAR1 antibody (Ab)-treated groups with isotype antibody-treated groups. (C) C57BL/6J mice ( $n = 5$ ) were immunized twice with 5  $\mu$ g of WH-01 RBD protein and 5 nmol AMP-dT<sub>50</sub>. Mice received IFNAR1 blocking antibody or isotype control intraperitoneally 1 day prior to each dose. (D) IFNAR-KO mice ( $n = 4$ ) and IFNAR-wild-type (WT) mice (C57BL/6J,  $n = 4$ ) were immunized twice with 5  $\mu$ g of OVA protein and 5 nmol AMP-dT<sub>50</sub>. (C and D) Cells were assayed 7 days post-booster dose. Flow cytometry analysis of cytokine production by CD8<sup>+</sup> T cells in peripheral blood upon restimulation with SIINFEKL peptide (C) or RBD OLPs (D). Mock-immunized animals received PBS vehicle only. Values depicted are means (SD). \* $P < 0.05$ ; \*\* $P < 0.01$ ; \*\*\* $P < 0.001$ ; \*\*\*\* $P < 0.0001$ , one-way ANOVA followed by Tukey's post hoc analysis (A to C) or unpaired  $t$  test (D).

than in AMP groups and, despite exhibiting detectable cytokine up-regulation over baseline, did not reach sufficient levels to induce effective downstream immune induction (Fig. 1).

Of particular note is the strong AMP-DNA-mediated induction of IFN-I, an important mediator of robust immune activation following initial pathogen detection (36, 37). To investigate its impact on AMP-DNA-induced immune activation, IFNAR1, essential for IFN-I signaling, was blocked in mice using an anti-IFNAR1 antibody 24 hours prior to immunization with WH-01 RBD and AMP-dT<sub>50</sub> (Fig. 7B). This resulted in nearly complete abrogation of the

consequent immune response. Assessment of cytokine levels in draining LNs revealed a significant reduction in almost all analytes measured compared to mice treated with an isotype control antibody (Fig. 7B and fig. S18, A to D), leading to a significantly attenuated T cell response in spleen, peripheral blood, and perfused lung (Fig. 7C and fig. S18, E to H). Only the humoral response was relatively unaffected by IFNAR1 blockade as determined by antibody titers to WH-01 RBD (fig. S18I). Similar results were observed in mice immunized with AMP-dA:dT<sub>50</sub> (fig. S19). The pivotal role of IFN-I signaling in AMP-DNA-induced immune responses was

corroborated in experiments using IFNAR-knockout (KO) mice, in which the adaptive immune response was nearly entirely abolished compared to IFNAR-sufficient mice (Fig. 7D). Overall, these data demonstrate that AMP-DNA adjuvants induce an LN environment rich in numerous proinflammatory cytokines, of which IFN-I plays a critical role in conducting the AMP-DNA signal leading to adaptive immunity.

### AMP-DNA adjuvants require TBK1 signaling

Strong IFN-I responses can be induced upon nucleic acid detection by intracellular or endosomal PRRs (37). In general, the major PRR pathways that detect nucleic acids are the inflammasome, which controls the proteolytic maturation of IL1 and IL18 via receptors such as absent in melanoma 2 (AIM2); various cytosolic sensors for DNA [e.g., cGas, interferon-gamma inducible protein 16 (IFI16), and DNA-dependent activator of interferon-regulatory factors (DAI)] and RNA (MDA5 and RIG-I) that signal through STING and MAVS, respectively, and activate TBK1/interferon regulatory factor (IRF) and I $\kappa$ B kinase (IKK)/nuclear factor  $\kappa$ B (NF $\kappa$ B); and endosomal TLRs that signal through MyD88 or TIR-domain-containing adapter-inducing interferon  $\beta$  (TRIF) and can also culminate in TBK1 and IKK pathways (38–41). The TBK1/IRF axis is the predominant regulator of IFN-I transcription. To determine whether AMP-DNA-induced immune activation relies on TBK1 signaling, TBK1-floxed mice expressing Cre-recombinase under the hematopoietic cell-specific *Vav1* promoter were immunized twice with OVA and AMP-dT<sub>50</sub>. Mice with TBK1 deletions in the hematopoietic compartment (TBK1<sup>fl/fl</sup>Vav-iCre) displayed a significantly diminished ability to generate splenic IFN $\gamma$  SFCs (Fig. 8A) and showed significantly reduced frequencies of circulating cytokine<sup>+</sup> CD8<sup>+</sup> T cells (Fig. 8B), indicating that AMP-DNA requires TBK1 signaling to induce cellular immune responses. To further elucidate which of the above-mentioned sensors upstream of TBK1 are responsible for AMP-DNA detection, a number of PRR-pathway KO mouse models were immunized with AMP-DNA and antigen. STING-KO mice did not exhibit a significant decrease in cytokine-producing CD8<sup>+</sup> T cells

compared to STING-sufficient comparator mice (fig. S20A) and displayed a similar proteomic inflammatory milieu in their LNs (fig. S20B). In contrast, deletion of *Unc93b1*, crucial for the correct expression of endosomal TLRs such as TLR3/7-9/11-13 (42) and known to lead to herpes simplex encephalitis in deficient individuals (43), resulted in a 52% decrease in circulating CD8<sup>+</sup> T cells that secreted TNF $\alpha$  and IFN $\gamma$  (Fig. 8C). TLR9 deletion resulted in a 23% reduction in cytokine response from CD8<sup>+</sup> T cells, which did not fully recapitulate *Unc93b1* deletion, suggesting that perhaps other TLRs could be involved in AMP-DNA sensing (Fig. 8D). Furthermore, deletion of MAVS also led to a significant, albeit smaller attenuation of the immune response, reducing the number of cytokine-secreting CD8<sup>+</sup> T cells by 21% (Fig. 8E), whereas AIM2 deletion showed no effect (fig. S20, C and D). Overall, these data suggest that AMP-DNA adjuvants may primarily be sensed by endosomal TLRs but could potentially use secondary pathways that involve transcription by RNA polymerase III and signaling through MAVS. These pathways then culminate in the activation of TBK1, which is able to induce potent IFN-I responses in APCs, and consequently stimulate strong adaptive immunity.

### DISCUSSION

Highly purified, recombinant subunit antigens yield remarkably safe and precise, albeit often poorly immunogenic, vaccines that require the presence of potent adjuvants to enhance their immunogenicity. Notable unadjuvanted exceptions include virus-like particle vaccines made from proteins that self-assemble into multimeric and highly immunogenic viral structures (44), conjugate vaccines that link polysaccharide antigens to carrier proteins such as tetanus or diphtheria toxoid that support T cell helper functions (45, 46), and, rarely, antigens that are sufficiently immunogenic to generate appropriate immune responses unaided (1, 2). However, responses to most of these vaccine classes are predominantly antibody-mediated, and immunity to the latter is improved by the addition of adjuvant (47, 48). Therefore, the next generation of adjuvant systems will

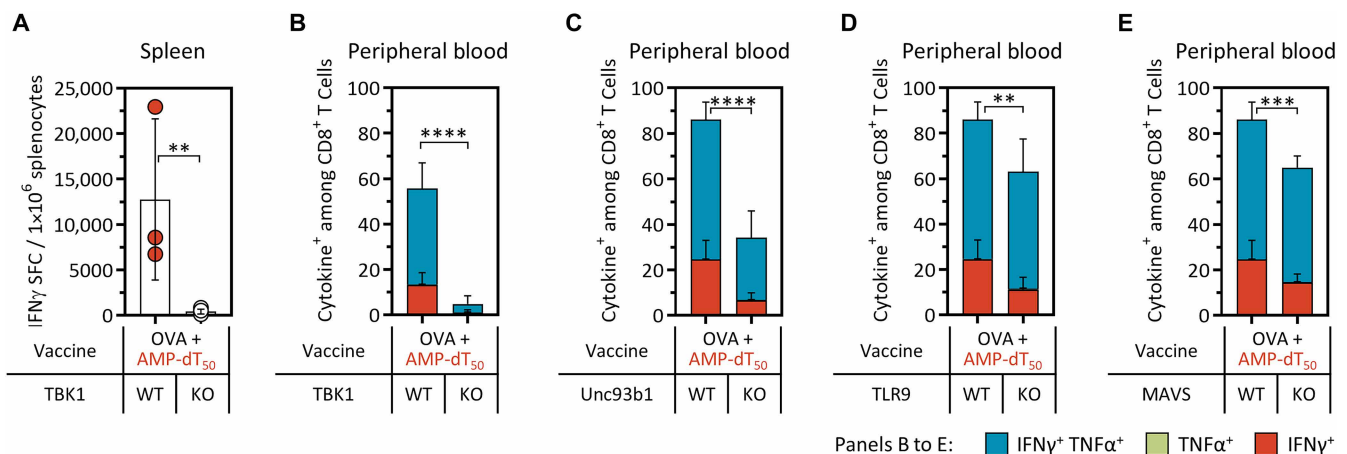


**Fig. 8. AMP-DNA requires TBK1 for signal transduction and may be sensed by endosomal TLRs as well as cytosolic RNA sensors.** Mice were immunized twice with 5  $\mu$ g of OVA protein and 5 nmol AMP-dT<sub>50</sub> as shown in Fig. 1C. Cells were restimulated ex vivo with SIINFEKL peptide on day 7 post-boost dose. (A and B) TBK1<sup>fl/fl</sup>Vav-iCre<sup>-/-</sup> mice (TBK1-KO,  $n = 6$ ) and TBK1<sup>fl/fl</sup>Vav-iCre<sup>-/-</sup> mice (TBK1-WT,  $n = 3$ ). (C) *Unc93b1*-KO mice ( $n = 5$ ) and C57B/6J mice (*Unc93b1*-WT,  $n = 9$ ). (D) TLR9-KO mice ( $n = 5$ ) and C57B/6J mice (TLR9-WT,  $n = 9$ ). (E) MAVS-KO mice ( $n = 5$ ) and C57B/6J mice (MAVS-WT,  $n = 9$ ). (A) ELISpot analysis of IFN $\gamma$  production in splenocytes. Shown is the frequency of IFN $\gamma$  SFCs per 10<sup>6</sup> splenocytes. (B to E) Flow cytometry analysis of cytokine production by CD8<sup>+</sup> T cells in peripheral blood. Shown are percentages of cytokine<sup>+</sup> cells among CD8<sup>+</sup> T cells. Values depicted are means (SD). \* $P < 0.05$ ; \*\* $P < 0.01$ ; \*\*\* $P < 0.001$ ; \*\*\*\* $P < 0.0001$ , unpaired  $t$  test.

need to combine several important capabilities to be most effective: (i) To increase bioavailability and durable immune activation while minimizing reactogenicity, vaccines will benefit from a targeted approach that delivers adjuvants directly to LNs where critical immune cells reside; (ii) to induce potent immunostimulation, especially activation of IFN-I crucial for antiviral and antitumor immunity (49, 50), adjuvants will need to access endosomal TLRs or cytosolic PRRs, which are known to strongly induce these activation pathways (4); (iii) last, a balanced cellular and humoral immune response is critical to achieve comprehensive immunity. To generate robust CD8<sup>+</sup> cytotoxic T lymphocyte responses, new adjuvants must also promote cross-presentation within APCs (51). In this study, we have engineered a class of DNA adjuvants, most prominently represented by AMP-dT<sub>50</sub>, that exhibits all three of these traits, exemplifying the potential gains in activity and tolerability that AMP modification can provide.

Consistent with prior studies, AMP modification of candidate DNA sequences resulted in efficient and targeted delivery to draining LNs corresponding with improved immunogenicity and favorable safety. In contrast, most immunostimulatory PRR/TLR agonists, such as small molecules or short nucleic acid sequences, fail to efficiently accumulate in immunorelevant tissues because of generally disadvantageous physicochemical characteristics (e.g., size <20 kDa) (13). This results in poor immunogenicity despite their inherent potential to activate the innate immune system. Consequently, delivery platforms are required to increase bioavailability and, in turn, potency. AMP conjugation of immunostimulatory adjuvants provides a simple and versatile strategy to guide vaccine components via tissue albumin-mediated shuttling from the injection site directly to draining LNs where they activate APCs (23, 24). Moreover, the association of AMP constructs with albumin is known to protect payloads from degradation and prolong bioavailability (24, 52). Here, we have demonstrated that AMP conjugation significantly enhances immunostimulatory properties of candidate DNA adjuvants, such as dT<sub>50</sub>, dA:dT<sub>50</sub>, HSV<sub>60</sub>, and ISD upon prime-boost administration. In mice, production of cytokines from splenic, lung-resident, and circulating antigen-specific T cells was increased multiple dozen- to hundred-fold when compared to SOL DNA adjuvants or clinical adjuvant comparators, which achieve limited LN accumulation. In parallel, antibody responses to AMP-DNA equaled that of classical depot-forming adjuvants, which are known to primarily elicit humoral responses. However, AMP-DNA adjuvants produced stronger T<sub>H</sub>1-associated IgG<sub>2c</sub> titers that likely play a supportive role in facilitating the significant cellular response present in these animals. Furthermore, NHPs treated with AMP-dT<sub>50</sub> and RBD antigen exhibited neutralizing antibody titers that exceeded those of convalescing patients who had recently recovered from SARS-CoV-2 infection. The notable immunogenicity-enhancing properties of these AMP adjuvants align with previous reports using AMP-CpG-7909 in vaccines targeting SARS-CoV-2 (26, 27) and Epstein-Barr virus (53). Furthermore, a recent clinical trial with AMP-CpG-7909 in KRAS-mutated pancreatic and colorectal cancer patients (28, 29) showed that targeted delivery of vaccine components can promote favorable immunogenicity and clinical efficacy while avoiding systemic toxicity. Treatment-emergent adverse events were limited to grades 1 to 2; no dose-limiting toxicity or cytokine-release syndrome was observed. Concurrently, 84% of patients overall and 100% of those treated at the recommended phase 2 dose showed mKRAS-specific T cell responses *ex vivo*, which strongly associated with tumor biomarker

responses and decreased risk of progression and death. Overall, these data demonstrate that targeted delivery not only increases the potency of vaccines by concentrating their components in immunorelevant tissues but can also prevent harmful side effects.

Second, for adjuvants to be effective immunostimulators, they must gain access to and interact with the appropriate PRRs within cells. APCs express a myriad of cytosolic and endosomal sensors and are strong inducers of IFN-I signaling pathways (37). Localized IFN-I production in the LNs ensures proper activation of not only APCs themselves, but also CD8<sup>+</sup> T cells (49, 50), which in turn facilitates adaptive responses against cancers (54) and intracellular pathogens such as viruses (55), tuberculosis (56), and malaria (8, 57). This makes these APC-associated, nucleic acid-sensing PRRs desirable targets for new adjuvants. In this study, we have engineered PS-stabilized DNA and explored various design characteristics to optimally stimulate the local immune system within the LNs. This was demonstrated by the significant induction of IFN-I and inflammatory transcripts in the LNs, including multiple cytosolic PRRs and TBK1, antigen processing and presentation machinery, APC activation markers and costimulatory receptors, as well as the subsequent increased secretion of various cytokines and chemokines. IFN-I played a pivotal role in initiating adaptive immunity, as IFNAR1 blockade or knockout abrogated all cellular responses, in agreement with previous studies (49). Crucially, however, to reach these cytosolic and endosomal receptors, adjuvants must first be efficiently endocytosed and, in the case of cytosolic PRRs, also escape the endocytic pathway to enter the cytosol and avoid entrapment and eventual degradation within the lysosome, a rate-limiting step that determines the efficacy of many therapeutics (58). The diacyl lipid constituent of the AMP modification could facilitate these mechanisms to allow AMP-DNA adjuvants to engage TBK1-mediated pathways. AMP constructs have demonstrated the ability to insert into lipid bilayers or form micellar structures (23), either of which could potentially enhance initial APC uptake and/or facilitate the disruption of endosomal membranes to allow endosomal escape (59). The exact mechanisms require further investigation; however, SOL dT<sub>50</sub> was unable to initiate notable immune responses, despite sufficiently accumulating in the LNs during fluorescent *in vivo* imaging studies, suggesting that AMP modification is critical for successful immune induction after the adjuvant accumulates in the LNs. Overall, the data suggest that AMP-DNA adjuvants are strong inducers of critical IFN-I signals needed to promote cellular immunity and that AMP modification not only facilitates delivery to the LNs but may enhance conjugated vaccine payload access to intracellular PRRs.

Last, improved vaccine potency depends in part on cross-presentation of antigens to generate robust populations of cytotoxic effector and memory T cells. Cellular immunity is an essential component of protection against infected or transformed cells and operates in synergy with a parallel humoral response. However, most vaccines in use today that do not contain live-attenuated or inactivated (self-adjuncting) vectors primarily elicit antibody responses (5, 60, 61). In isolation, these are often insufficient to provide adequate protection against diseases caused by many intracellular pathogens or cancer, which instead require combined humoral and cellular immunity (62). For example, neutralizing antibodies were not sufficient to protect patients against fatal SARS-CoV-2 infection, suggesting that cellular responses are required for comprehensive protection against this virus (63). Moreover, antibody responses in the presence

of inadequate innate immune activation and thus lack of T helper cell participation are generally short-lived; most responses to SARS-CoV-2 vaccine begin to wane significantly within 3 to 6 months after vaccination (64–66). Thus, to achieve appropriate APC activation that stimulates potent humoral responses, while simultaneously promoting robust and durable cellular immunity, new adjuvants will ideally induce strong IFN-I signaling, which enhances their intrinsic cross-presentation and costimulatory capabilities (67, 68), resulting in strong CD8<sup>+</sup> T cell priming and memory generation (18, 69). AMP-DNA adjuvants demonstrated effective activation of antigen-specific CD8<sup>+</sup> T cell populations in secondary lymphoid and peripheral tissues as well as in circulation. This was accompanied by significantly elevated production of IFN-I, and the enhanced transcription of genes important for cross-presentation. Of note, transporter associated with antigen processing 1 (*Tap1*), TAP-binding protein (*Tapbp*), and proteasome subunits (*Psmb9/10*), all crucial in the cytosolic pathway of cross-presentation (67), as well as cathepsins (*Ctss* and *Ctsc*) involved in the vacuolar pathway of cross-presentation (70, 71), were transcriptionally up-regulated in LNs upon vaccination with AMP-DNA adjuvants. Together, these findings indicate an ability of AMP-DNA adjuvants to potentially induce cellular immune responses facilitated by significant production of IFN-I and the promotion of cross-presentation of antigens via major histocompatibility complex I (MHC I) molecules.

In light of the present scarcity of approved T cell-inducing adjuvants that fulfill the abovementioned criteria, it is prudent to invest in the development of new immunostimulators. While the first-generation AMP adjuvant, AMP-CpG-7909, is currently being evaluated in the clinic and has so far shown a favorable safety profile and the ability to induce notable antitumor T cell responses in patients (28, 29), the development of further AMP-DNA adjuvants aims to generate new classes of immunostimulators with potentially distinct signaling pathways that could be used either in synergy or as substitutes, depending on the particular indication, treatment objectives, and patient group of interest. While AMP-CpG mainly signals through the unmethylated CpG motif-specific receptor, TLR9, whose expression in humans is thought to be mostly limited to plasmacytoid DCs and B cells (72, 73), AMP-DNA may engage more ubiquitous endosomal or cytosolic PRRs. Ideally, a suite of adjuvants would exist with various activity profiles to select from, which could be tailored to the goals of the immunotherapy of each indication.

We are aware of some limitations in the current study. While immunogenicity data obtained from NHP ( $n = 3$ ) corroborate the notable responses obtained in mice and suggest the potential of AMP-DNA as an additional example of efficacious and safe AMP-adjuvant systems for use in humans, larger studies will be useful to support more decisive conclusions about its potential clinical utility. While the magnitude of T cell responses induced by AMP-DNA in NHPs is reduced compared to murine levels, this may reflect the greater diversity of immune background present in outbred rhesus macaques and/or less optimal antigen-encoded immune epitopes; systematic optimization of dose, regimen, antigen, and route of immunization in NHPs may lead to improved responses. While some insights into AMP-DNA adjuvant mediated signal transduction have been gained, such as the involvement of the TBK1-IFN-I signaling axis and potential involvement of Unc93b1-associated TLRs, these initial findings will need to be substantiated by more detailed analysis of the exact mechanisms and proteins involved to precisely

define how AMP-DNA adjuvants are sensed and how they shape the downstream immune response. Further investigation is needed to determine the mechanisms of cytosolic entry and participation of critical immune cell lineages. Last, this study is currently limited to immunogenicity data upon vaccination with AMP-DNA adjuvants and should be complemented by further pathogen or tumor challenge studies that can determine the adjuvant effect on vaccine efficacy.

In summary, AMP-DNA represents a class of potent and safe immunostimulatory adjuvants that generate substantial humoral and cellular immunity to coadministered protein subunit antigens. Strong immunogenicity is associated with adjuvant design parameters facilitating direct targeting of the innate immune system within LNs, stimulation of TBK1-mediated nucleic acid sensor pathways, and induction of potent IFN-I responses. These and previous findings suggest that AMP-conjugated adjuvants, such as AMP-DNA and AMP-CpG-7909, are promising candidate vaccine adjuvants for clinical use in infectious disease and cancer.

## MATERIALS AND METHODS

### Experimental design, animals, and tissue processing

All animal studies were approved by the Institutional Animal Care and Use Committees at New Iberia Research Center (protocol no. 2020-8738-022), Charles River Accelerator and Development Laboratories (protocol no. 2021-1259), and the University of Massachusetts Chan School of Medicine (protocol no. 2022-00019) and followed federal, state, and local guidelines for the care and use of animals. For mouse studies, female 6- to 8-week-old C57BL/6J and B6.129S2-Irfar1<sup>tm1Agt</sup>/Mmjax mice (referred to as IFNAR-KO mice) were purchased from The Jackson Laboratory (Bar Harbor, ME). B6-TBK1<sup>fl/fl</sup> mice were generated by Millennium Pharmaceuticals (Takeda) and crossed with Vav-iCre mice to generate offspring with TBK1 deletions specifically in the hematopoietic compartment (referred to as TBK1-KO). STING-KO mice were acquired from the G. Barbers laboratory at the University of Miami and backcrossed onto the C57BL/6J background (74). Goldenticket mice (designated STING<sup>-/-</sup> to distinguish from STING-KO mice) were purchased from The Jackson Laboratory. Unc93b1-KO mice were generated as part of the Knockout Mouse Project (KOMP ID VG10049) by the E. Latz laboratory at Regeneron Pharmaceuticals, Inc. (Tarrytown, NY) (75). MAVS-KO mice were acquired from the Z. Chen laboratory at the Howard Hughes Medical Institute (76). AIM2-KO mice on C57BL/6J background were obtained from Genentech (San Francisco, CA) (77) and crossed with STING-KO mice to produce STING/AIM2 double KO mice. TLR9-KO mice were generated by the S. Akira laboratory at Osaka University (78). The indicated antigen/adjuvant combinations were administered into mice subcutaneously at the base of the tail (bilaterally, 50  $\mu$ l each) at weeks 0 and 2. Spleen and perfused lung samples were collected 7 days post-booster dose. Splens were processed into single-cell suspensions, and red blood cells were lysed in Ammonium-Chloride-Potassium (ACK) lysis buffer (Quality Biological Inc., catalog no. 118156101). Lungs were harvested following perfusion with 10 ml of phosphate-buffered saline (PBS) into the right ventricle of the heart. Perfused lung tissue was physically dissociated and digested with RPMI 1640 media containing collagenase D (1 mg/ml) and deoxyribonuclease I (25 U/ml). Peripheral blood samples were collected retro-orbitally at the indicated time points and processed for PBMCs and serum. LN samples were

collected at 2, 6, 24, and 72 hours post–primary dose for transcriptome analysis, and 6 and 24 hours post–primary dose for proteomic analysis.

For NHP studies, animals were housed at New Iberia Research Center (New Iberia, LA). Three outbred, Indian-origin, 4- to 5-year-old female rhesus macaques (*Macaca mulatta*) received immunizations subcutaneously into the upper thighs at weeks 0 and 4 for evaluation of T cell and antibody responses. Blood samples were obtained at baseline and throughout the study in 2-week intervals and were then processed for PBMCs and serum. LNs were sampled via FNA at baseline and weeks 2 and 6, and analyzed for GC B cell specificity. For analysis of the inguinal LN transcriptome, FNAs were collected 24 and 48 hours after a third dose at week 10.

### Vaccine components

For mouse studies, vaccines consisted of 5  $\mu$ g of SARS-CoV-2 Spike RBD WH-01 (RBD) protein (GenScript, catalog no. Z03483) or 5  $\mu$ g of OVA protein (InvivoGen, catalog no. vac-pova), combined with 5 nmol DNA adjuvant. The adjuvants included AMP-dA:dT, AMP-dT, and any of their length, sequence, or linkage variants as well as their soluble counterparts (SOL dA:dT and SOL dT) as indicated. AMP-CpG-7909 was used at 1 nmol per injection. All were synthesized by AxoLabs GmbH (Germany). Comparator adjuvants included Alhydrogel adjuvant 2% (alum, 100  $\mu$ g, InvivoGen, catalog no. vac-alu), AS03-like squalene-based adjuvant (AddaS03, 1:2 dilution, InvivoGen, catalog no. vac-as03), MPLA (10  $\mu$ g, InvivoGen, catalog no. vac-mpla), MF59-like adjuvant (AddaVax, 1:2 dilution, InvivoGen, catalog no. vac-adx), and IFA (1:2 dilution, InvivoGen, catalog no. vac-ifa). For fluorescence in vivo imaging studies, DNA adjuvants were 3'-conjugated to Cy5 fluorophore (AxoLabs). Mock treatment groups received a matching dose of antigen in the absence of adjuvant or were treated with vehicle alone (PBS), as indicated. For NHP studies with rhesus macaques, vaccines consisted of 140  $\mu$ g of SARS-CoV-2 Spike RBD WH-01 protein admixed with 5 mg of AMP-dT<sub>50</sub>.

### DNA adjuvant synthesis

Single-stranded phosphorothioated 2'-deoxyoligonucleotides were synthesized according to the conventional solid-phase oligonucleotide synthesis technology using standard phosphoramidite-based oligomerization chemistry. Oligonucleotides were assembled on solid support using a Mermade 12 synthesizer (LGC Bioautomation) controlled by the Poseidon software package (version 2.7.0.0). To introduce PS linkages, a 100 mM solution of 3-amino-1,2,4-dithiazole-5-thione dissolved in acetonitrile (ACN)–pyridine (2:3, v/v) was used as sulfurizing agent. Diacyl-lipid phosphoramidite coupling was performed using 5-(Ethylthio)-1H-tetrazole (ETT; 500 mM) formulated in isobutyronitrile-dichloromethane (DCM; 1:1, v/v). Oligonucleotides were cleaved from the solid support with concomitant removal of all protecting groups using aqueous ammonia and aqueous methylamine (AMA; 1:1, v/v mixture of concentrated aqueous ammonia and 40% aqueous methylamine) with shaking at 25°C. Samples were then dried under reduced pressure (SpeedVac concentrator, Thermo Fisher Scientific) and were finally reconstituted in 100 mM aqueous triethylammonium acetate (TEAAc) to yield crude sample solutions for subsequent purification. Crude preparations were purified by preparative reversed-phase high-performance liquid chromatography (RP-HPLC) using an XBridge BEH C18 [19  $\times$  50 mm, Optimum Bed Density (OBD), 5- $\mu$ m particle] column available

from WATERS on an ÄKTA Pure 100 system (Cytiva). Eluent A was 100 mM triethylammonium acetate (TEAA) (pH 7) in water, and eluent B was a formulation of eluent A in 95% acetonitrile-water. Ultraviolet (UV) traces at 260 and 280 nm were recorded to monitor product elution. Appropriate fractions were pooled and precipitated overnight in the freezer using 3 M NaOAc (pH 5.2) in ethanol (1:32, v/v). Pellets were collected by centrifugation and reconstituted in purified water. 4,4'-Dimethoxytrityl (DMT)–On oligos were thereafter detritylated by treatment with 10% acetic acid, followed by repurification on the same RP-HPLC system. The purified complementary DNA single strands were mixed in an equimolar ratio and annealed by heating to 70°C for 5 min followed by cooling to 25°C in 2 hours. The resultant DNA duplexes were characterized by non-denaturing HPLC to evaluate their purity (duplex purity >90%, as per integration of the UV signal at 260 nm of the analytical non-denaturing HPLC trace). HPLC-purified DNA single strand equipped with a 3'-aminohexyl linker was conjugated to a sulfo-Cy5 *N*-hydroxysuccinimide (NHS) ester (Lumiprobe). Samples were quantified by measuring the UV absorption at 260 nm (based on the theoretical extinction coefficient, computed by the nearest neighbor method and the molecular weight of the sodium salt). Samples were analyzed for purity and identity using liquid chromatography–mass spectrometry.

### Restimulating peptides

For ex vivo restimulation of cells from animals immunized with RBD antigen, custom 15-mer OLPs with 11-amino acid overlap were generated spanning the SARS-CoV-2 Spike RBD WH-01 protein (amino acids Arg<sup>319</sup>-Ser<sup>591</sup>, GenScript). WH-01 peptides that contained VOC mutation loci were substituted with the corresponding mutant sequences when applicable. Ex vivo restimulation of cells from animals that were immunized with OVA antigen was performed with PepTivator Ovalbumin OLP (Miltenyi, catalog no. 130-099-771) or SIINFEKL peptide (AnaSpec Inc., catalog no. AS-60193-1).

### Cytokine production analysis by flow cytometry to assess T cell activation

For vaccine immunogenicity studies in mice, ICS was performed for TNF $\alpha$  and IFN $\gamma$ . Peripheral blood cells and lung-resident lymphocytes (10<sup>6</sup> cells per well) were collected 7 days after the booster dose and stimulated overnight (16 to 20 hours) with peptides (2  $\mu$ g per peptide per ml) at 37°C, 5% CO<sub>2</sub> in the presence of brefeldin A (3  $\mu$ g/ml; Invitrogen, catalog no. 00-4506-51) and monensin (2  $\mu$ M; BioLegend, catalog no. 420701). A Live/Dead fixable cell stain (Aqua, Invitrogen, catalog no. L34966) was used to evaluate viability of the cells during flow cytometry. Cells were surface-stained with antibodies against anti-mouse CD4 [phycoerythrin (PE)–Cy7, clone: GK1.5, Invitrogen, catalog no. 25-0041-82, 1:200 dilution] and anti-mouse CD8a (APC, clone: 53-6.7, eBioscience, catalog no. 17-0081-83, 1:200) and subsequently fixed and permeabilized with BD CytoFix/CytoPerm (BD, catalog no. 554714). Cells were further stained intracellularly with antibodies against anti-mouse IFN $\gamma$  (PE, clone: XMG1.2, BD, catalog no. 554412, 1:200), anti-mouse TNF $\alpha$  [fluorescein isothiocyanate (FITC), clone: MP6-XT22, BD, catalog no. 554418, 1:200], and anti-mouse CD3 (APC-Cy7, clone: 17A2, BD, catalog no. 560590, 1:200). Phorbol 12-myristate 13-acetate (PMA; 50 ng/ml) and ionomycin (1  $\mu$ M) were used as positive control, and complete medium plus DMSO (at peptide equivalent volume) was used as the

negative control. Sample acquisition was performed on FACSCanto II (BD), and data were analyzed with FlowJo V10 software (BD).

For NHP studies, frozen PBMCs were thawed and rested overnight. A total of  $10^6$  PBMCs per well were resuspended in R10 media supplemented with anti-human CD49d monoclonal antibody (clone: 9F10, BD, catalog no. 555502), anti-human CD28 monoclonal antibody (clone: CD28.2, BD, catalog no. 555726), and Golgi inhibitors monensin (Thermo Fisher Scientific, catalog no. NC0176671) and brefeldin A (Thermo Fisher Scientific, catalog no. 50-112-9757) and incubated at 37°C for 8 hours, then maintained at 4°C overnight. The next day, cells were surface-stained with antibodies against anti-human CD4 (PE-Cy5.5, clone: S3.5, Invitrogen, catalog no. MHCD0418, 1:100), anti-human CD8 (AF647, clone: RPA-T8, BioLegend, catalog no. 301022, 1:400), and Live/Dead dye (Aqua, Invitrogen, catalog no. L34966) and subsequently fixed with BD CytoFix/CytoPerm (BD, catalog no. 554714). Cells were further stained intracellularly with antibodies against anti-human CD3 (APC-Cy7, clone: SP34-2, BD, catalog no. 557757, 1:200), anti-human IFN $\gamma$  (AF700, clone: B27, BioLegend, catalog no. 506516, 1:400), anti-human IL2 (BV421, clone: MQ1-17H12, BioLegend, catalog no. 500328, 1:20), and anti-human TNF $\alpha$  (BV605, clone: MAb11, BioLegend, catalog no. 502936, 1:20). Stained cells were fixed in 1.5% formaldehyde and acquired on a BD FACS Symphony. Data were analyzed with BD FlowJo V10 software.

#### Mouse antigen-specific tetramer staining to assess antigen-specific T cells

MHC-tetramer staining on freshly isolated, unstimulated mouse peripheral blood samples was performed using an OVA-PE iTag tetramer specific for sequence SIINFELK (MBL, catalog no. TB-5001-1) or RBD-PE tetramer specific for sequence VNFNFNGL (NIH Tetramer Core Facility), and antibodies against anti-mouse CD8a (APC, clone: 53-6.7, eBioscience, catalog no. 17-0081-83, 1:200), anti-mouse CD3 (APC-Cy7, clone: 17A2, BD, catalog no. 560590, 1:200). A Live/Dead fixable cell stain (Aqua, Invitrogen, catalog no. L34966) was used to evaluate viability of the cells during flow cytometry. Sample acquisition was performed on a BD FACSCanto II, and data were analyzed with BD FlowJo V10 software.

#### NHP antigen-specific GC B cell analysis in LN FNAs

Biotinylated RBD protein (Acro Biosystems, catalog no. SPD-C82E9) was complexed with fluorochrome-conjugated streptavidin APC (BioLegend, catalog no. 405207). LN cells from FNA were incubated with the RBD-fluorochrome complex and subsequently stained with Live/Dead dye (Aqua, Invitrogen, catalog no. L34966), anti-human IgM (FITC, clone: G20-127, BD, catalog no. 555782, 1:5), anti-human IgG (PE-Cy7, clone: G18-145, BD, catalog no. 561298, 1:20), anti-human CD3 (AF700, clone: SP34-2, BD, catalog no. 557917, 1:20), anti-human PD-1 (BV650, clone: EH12.1, BD, catalog no. 564104, 1:20), anti-human CD20 (PE/Dazzle 594, clone: 2H7, BioLegend, catalog no. 302348, 1:20), anti-human CD4 (APC-Cy7, clone: OKT4, BioLegend, catalog no. 317418, 1:20), and anti-human CXCR5 (PerCP-eF710, clone: MU5UBEE, Thermo Fisher Scientific, catalog no. 46-9185-42, 1:20). Cells were fixed/permeabilized using Transcription Factor Staining Buffer Set (Thermo Fisher Scientific, catalog no. 00-5521-00) and further stained with anti-human Bcl-6 (PE, clone: 7D1, BioLegend, catalog no. 358504, 1:20) and anti-human Ki-67 (BV421, clone: 11F6, BioLegend, catalog no. 151208, 1:20). Sample acquisition was performed on

a BD FACS Symphony, and data were analyzed with BD FlowJo V10 software.

#### Enzyme-linked immunospot assay for IFN $\gamma$ to assess T cell activation

For mouse studies, precoated 96-well mouse IFN $\gamma$  enzyme-linked immunospot (ELISpot) plates (MabTech, catalog no. 3321-4HPW) were blocked with RPMI + 10% fetal bovine serum (FBS) for 2 hours at room temperature (RT). Mouse splenocytes ( $0.1 \times 10^6$ ) were plated into each well and stimulated overnight with RBD- or OVA-derived OLPs (2  $\mu$ g/ml per peptide). ELISpot assays were performed as instructed by the manufacturer.

For NHP studies, ELISpot assays were performed using Monkey IFN $\gamma$  ELISpotPLUS kits (MabTech, catalog no. 3241M-4HPW). Precoated 96-well ELISpot plates were blocked with RPMI + 10% FBS for 2 hours at RT. PBMCs ( $0.2 \times 10^6$ ) were plated into each well and stimulated overnight with RBD-derived OLPs for WH-01, Beta, and Delta variants (4  $\mu$ g/ml per peptide). The spots were developed based on the manufacturer's instructions. In both animal models, PMA (50 ng/ml) and ionomycin (1  $\mu$ M) were used as positive controls, and RPMI + 10% FBS with DMSO was used as the negative control. Spots were scanned and quantified using an S6 ImmunoSpot analyzer (CTL).

#### FluoroSpot assay for IFN $\gamma$ , TNF $\alpha$ , and IL2 to assess T cell activation

Precoated 96-well mouse IFN $\gamma$ /TNF $\alpha$ /IL2 FluoroSpot plates (MabTech, catalog no. FSP-414245) were blocked with RPMI + 10% FBS for 2 hours at RT. Mouse splenocytes ( $0.1 \times 10^6$ ) were plated into each well and stimulated overnight with RBD- or OVA-derived OLPs (2  $\mu$ g/ml per peptide). FluoroSpot assays were performed as instructed by the manufacturer.

#### Multiplexed proteomics (Luminex) to assess T cell activation

To determine cytokine production from T cells, mice were immunized twice, and spleens were stimulated overnight with OLPs 7 days after booster dose. Cell culture supernatant was diluted 1:2 (TNF $\alpha$ , IL2, and GM-CSF) or 1:20 (IFN $\gamma$  and GzmB) and assayed using the MCD8MAG-48K kit (EMD Millipore). The assay was performed as instructed by the manufacturer.

#### LN proteomics

To determine the cytokine/chemokine content of mouse LNs, animals were vaccinated once, and inguinal LNs were collected 6 to 48 hours postimmunization. For IFNAR-1 blockade, 870  $\mu$ g of an antagonistic monoclonal antibody (clone: MAR1-5A3, BioXcell, catalog no. BE0241) or an isotype control (clone: MOPC-21, BioXcell, catalog no. BE0083) were injected intraperitoneally 24 hours prior to immunization. Protein Extraction Buffer (Invitrogen, catalog no. EPX-9999-000) containing Mini protease inhibitor cocktail (Roche, catalog no. 53945000) and HALT phosphatase inhibitors (Thermo Fisher Scientific, catalog no. 78442) was added to the intact LNs prior to homogenization using a TissueLyser II (QIAGEN). Centrifugation-cleared lysates were analyzed with Luminex Cytokine and Chemokine kits (EMD Millipore, catalog no. MCYTOMAG-70K and MECY2MAG-73K).

#### ELISA for antibody titers

ELISAs were performed to determine antigen-specific antibody titers in serum. For murine studies, ELISA plates were coated with

OVA (200 ng per well; InvivoGen, catalog no. vac-pova) or RBD antigen (200 ng per well; GenScript, catalog no. Z03483) overnight at 4°C. Plates were preblocked with 2% bovine serum albumin for 2 hours at RT. Serially diluted mouse sera were transferred to the ELISA plates and incubated for 2 hours at RT. Plates were washed four times with washing buffer (BioLegend, catalog no. 4211601) and then incubated for 1 hour at RT with horseradish peroxidase (HRP)-conjugated anti-mouse secondary antibodies (1:2000 dilution) against either pan-IgG (Fc $\gamma$ ) (Jackson ImmunoResearch, catalog no. 315-035-046), IgG1 (Jackson ImmunoResearch, catalog no. 115-035-205), or IgG2c (Jackson ImmunoResearch, catalog no. 115-035-208). Plates were again washed four times with washing buffer, after which the plates were developed with 3,3',5,5'-tetramethylbenzidine for 10 min at RT, and the reaction was stopped with 1 N sulfuric acid. The absorbance at 450 nm was measured by an ELISA plate reader. Titers were determined at an absorbance cutoff of 0.5 OD (optical density).

For NHP assays, ELISA plates were coated with 100 ng per well of RBD WH-01, Beta, Delta, or Omicron antigen. The detection antibody used was HRP-conjugated goat anti-human IgG (H + L) (Thermo Fisher Scientific, catalog no. SA5-10283) at a 1:2000 dilution. The WHO International Standard for anti-SARS-CoV-2 immunoglobulin (anti-RBD IgG High 20/150, NIBSC) was used for reference values. Serum titers were determined at an absorbance cutoff of 0.5 OD and converted into BAU per milliliter using the WHO standard.

### SARS-CoV-2 pseudovirus neutralization assay for NHP sera

The SARS-CoV-2 pseudovirus assay was performed by Genecopoeia as previously described (27). SARS-CoV-2 Spike-pseudotype lentiviruses from the Washington 1 (WA1) D614G, Delta, and Omicron variants were used. Briefly, a human embryonic kidney (HEK) 293T cell line overexpressing angiotensin-converting enzyme 2 (ACE2) and transmembrane protease, serine 2 (TMPRSS2) was seeded at a density of  $1.2 \times 10^4$  cells per well overnight. Threefold serial dilutions of heat-inactivated serum samples were prepared and mixed with 50  $\mu$ l of pseudovirus. The mixture was incubated at 37°C for 1 hour before adding to the HEK293T-hACE2 cells. After 72 hours, the cells were lysed, and firefly luciferase activity was determined. SARS-CoV-2 neutralization titers were defined as the sample dilution at which a 50% reduction in relative light units (RLU) was observed relative to the average of the virus control wells. Convalescent plasma samples from patients who had recovered from SARS-CoV-2 infection (COVID-19) within 4 weeks of sample collection were obtained from US Biolab (Rockville, MD) and ALLCELLS (Alameda, CA). All samples were received and stored frozen at  $-80^\circ\text{C}$  until analysis.

### Gene transcript analysis by NanoString

For mouse studies, inguinal LNs were harvested from immunized C57BL/6J mice at the indicated time points, processed into single cell suspensions, and lysed with RLT buffer (QIAGEN, catalog no. 79216). Transcriptional profiles of immune signaling were generated using the nCounter Mouse Immunology Panel of 561 mouse immune response genes (NanoString Technologies, catalog no. XT-CSO-MIM1-12).

For NHP studies, LN FNAs were assessed using the nCounter NHP Immunology Panel of 770 macaque immune response genes (NanoString Technologies, catalog no. XT-CSO-NHPIMI-12). Transcriptional responses were assessed with nSolver software V4.0 (NanoString Technologies), and differential gene expression analysis was carried out using ROSALIND software (Rosalind, Inc.).

### Biodistribution analysis by IVIS

C57BL/6J mice were immunized once with 5  $\mu$ g of WH-01 Spike RBD protein and 5 nmol Cy5-labeled DNA adjuvant. "No Cy5" control animals were administered antigen plus unlabeled AMP-DNA. Six hours and 1, 3, 5, and 7 days postinjection, inguinal LNs were harvested and imaged ex vivo using the IVIS Spectrum (PerkinElmer, Waltham, MA).

### Statistics

For comparing two experimental groups, two-tailed *t* test analysis was used when normal distribution and homogeneity of variance, determined by Levene's test, were established. Where these assumptions did not apply, the Mann-Whitney test was used instead. For comparison of multiple groups, ordinary one-way analysis of variance (ANOVA) followed by Tukey's or Sidák's post hoc analysis, as indicated, was used to compare experimental groups. NanoString statistical analysis was performed using ROSALIND software.

### Supplementary Materials

#### The PDF file includes:

Figs. S1 to S20

Legend for data file S1

#### Other Supplementary Material for this manuscript includes the following:

Data file S1

### REFERENCES

1. E. E. Walsh, G. Pérez Marc, A. M. Zareba, A. R. Falsey, Q. Jiang, M. Patton, F. P. Polack, C. Llapur, P. A. Doreski, K. Ilangovan, M. Rämety, Y. Fukushima, N. Hussien, L. J. Bont, J. Cardona, E. DeHaan, G. Castillo Villa, M. Ingilizova, D. Eiras, T. Mikati, R. N. Shah, K. Schneider, D. Cooper, K. Koury, M.-M. Lino, A. S. Anderson, K. U. Jansen, K. A. Swanson, A. Gurtman, W. C. Gruber, B. Schmoel-Thoma, RENOIR Clinical Trial Group, Efficacy and safety of a bivalent RSV prefusion F vaccine in older adults. *N. Engl. J. Med.* **388**, 1465–1477 (2023).
2. M. M. J. Cox, P. A. Patriarca, J. Treanor, FluBlok, a recombinant hemagglutinin influenza vaccine. *Influenza Other Respi. Viruses* **2**, 211–219 (2008).
3. E. C. Lavelle, C. P. McEntee, Vaccine adjuvants: Tailoring innate recognition to send the right message. *Immunity* **57**, 772–789 (2024).
4. T. Zhao, Y. Cai, Y. Jiang, X. He, Y. Wei, Y. Yu, X. Tian, Vaccine adjuvants: Mechanisms and platforms. *Signal Transduct. Target. Ther.* **8**, 283 (2023).
5. S. A. Plotkin, Correlates of protection induced by vaccination. *Clin. Vaccine Immunol.* **17**, 1055–1065 (2010).
6. V. M. Vashishtha, P. Kumar, The durability of vaccine-induced protection: An overview. *Expert Rev. Vaccines* **23**, 389–408 (2024).
7. H. Jiang, Q. Wang, L. Li, Q. Zeng, H. Li, T. Gong, Z. Zhang, X. Sun, Turning the old adjuvant from gel to nanoparticles to amplify CD8<sup>+</sup> T cell responses. *Adv. Sci.* **5**, 1700426 (2018).
8. J. E. Epstein, K. Tewari, K. E. Lyke, B. K. L. Sim, P. F. Billingsley, M. B. Laurens, A. Gunasekera, S. Chakravarty, E. R. James, M. Sedegah, A. Richman, S. Velmurugan, S. Reyes, M. Li, K. Tucker, A. Ahumada, A. J. Ruben, T. Li, R. Stafford, A. G. Eappen, C. Tamminga, J. W. Bennett, C. F. Ockenhouse, J. R. Murphy, J. Komisar, N. Thomas, M. Loyevsky, A. Birkett, C. V. Plowe, C. Loucq, R. Edelman, T. L. Richie, R. A. Seder, S. L. Hoffman, Live attenuated malaria vaccine designed to protect through hepatic CD8<sup>+</sup> T cell immunity. *Science* **334**, 475–480 (2011).
9. P. E. Duffy, J. Patrick Gorres, Malaria vaccines since 2000: Progress, priorities, products. *NJP Vaccines* **5**, 48 (2020).
10. P. Andersen, J. S. Woodworth, Tuberculosis vaccines—Rethinking the current paradigm. *Trends Immunol.* **35**, 387–395 (2014).
11. I. Satti, H. McShane, Current approaches toward identifying a correlate of immune protection from tuberculosis. *Expert Rev. Vaccines* **18**, 43–59 (2019).
12. R. Arens, T. van Hall, S. H. van der Burg, F. Ossendorp, C. J. M. Melief, Prospects of combinatorial synthetic peptide vaccine-based immunotherapy against cancer. *Semin. Immunol.* **25**, 182–190 (2013).
13. N. L. Treviskis, L. M. Kaminskis, C. J. H. Porter, From sewer to saviour—Targeting the lymphatic system to promote drug exposure and activity. *Nat. Rev. Drug Discov.* **14**, 781–803 (2015).

14. M.-E. Fortier, S. Kent, H. Ashdown, S. Poole, P. Boksa, G. N. Luheshi, The viral mimic, polyinosinic:polycytidylic acid, induces fever in rats via an interleukin-1-dependent mechanism. *Am. J. Physiol. Regul. Integr. Comp. Physiol.* **287**, R759–R766 (2004).
15. C. Cunningham, S. Campion, J. Teeling, L. Felton, V. H. Perry, The sickness behaviour and CNS inflammatory mediator profile induced by systemic challenge of mice with synthetic double-stranded RNA (poly I:C). *Brain Behav. Immun.* **21**, 490–502 (2007).
16. J. P. Vasilakos, M. A. Tomai, The use of Toll-like receptor 7/8 agonists as vaccine adjuvants. *Expert Rev. Vaccines* **12**, 809–819 (2013).
17. S. M. Curley, D. Putnam, Biological nanoparticles in vaccine development. *Front. Bioeng. Biotechnol.* **10**, 867119 (2022).
18. J. Wang, S. Li, M. Wang, X. Wang, S. Chen, Z. Sun, X. Ren, G. Huang, B. D. Sumer, N. Yan, Y.-X. Fu, J. Gao, STING licensing of type I dendritic cells potentiates antitumor immunity. *Sci. Immunol.* **9**, ead3945 (2024).
19. L. Cao, P. Dong, J. Liu, J. Zhang, H. Xie, S. Yu, J. Zhang, Advancements in saponin-based vaccine adjuvants. *Med. Chem. Res.* **34**, 1817–1832 (2025).
20. D. J. Irvine, A. Aung, M. Silva, Controlling timing and location in vaccines. *Adv. Drug Deliv. Rev.* **158**, 91–115 (2020).
21. M. Abdallah, O. O. Müllertz, I. K. Styles, A. Mörsdorf, J. F. Quinn, M. R. Whittaker, N. L. Trevasakis, Lymphatic targeting by albumin-hitchhiking: Applications and optimisation. *J. Control. Release* **327**, 117–128 (2020).
22. P. Famta, S. Shah, N. Jain, D. A. Srinivasarao, A. Murthy, T. Ahmed, G. Vambhurkar, S. Shahrukh, S. B. Singh, S. Srivastava, Albumin-hitchhiking: Fostering the pharmacokinetics and anticancer therapeutics. *J. Control. Release* **353**, 166–185 (2023).
23. H. Liu, K. D. Moynihan, Y. Zheng, G. L. Szeto, A. V. Li, B. Huang, D. S. Van Egeren, C. Park, D. J. Irvine, Structure-based programming of lymph-node targeting in molecular vaccines. *Nature* **507**, 519–522 (2014).
24. K. D. Moynihan, R. L. Holden, N. K. Mehta, C. Wang, M. R. Karver, J. Dinter, S. Liang, W. Abraham, M. B. Melo, A. Q. Zhang, N. Li, S. Le Gall, B. L. Pentelute, D. J. Irvine, Enhancement of peptide vaccine immunogenicity by increasing lymphatic drainage and boosting serum stability. *Cancer Immunol. Res.* **6**, 1025–1038 (2018).
25. G. Zhu, G. M. Lynn, O. Jacobson, K. Chen, Y. Liu, H. Zhang, Y. Ma, F. Zhang, R. Tian, Q. Ni, S. Cheng, Z. Wang, N. Lu, B. C. Yung, Z. Wang, L. Lang, X. Fu, A. Jin, I. D. Weiss, H. Vishwasrao, G. Niu, H. Shroff, D. M. Klinman, R. A. Seder, X. Chen, Albumin/vaccine nanocomplexes that assemble in vivo for combination cancer immunotherapy. *Nat. Commun.* **8**, 1954 (2017).
26. M. P. Steinbuck, L. M. Seenappa, A. Jakubowski, L. K. McNeil, C. M. Haqq, P. C. DeMuth, A lymph node–targeted Amphiphile vaccine induces potent cellular and humoral immunity to SARS-CoV-2. *Sci. Adv.* **7**, eabe5819 (2021).
27. L. M. Seenappa, A. Jakubowski, M. P. Steinbuck, E. Palmer, C. M. Haqq, C. Carter, J. Fontenot, F. Villinger, L. K. McNeil, P. C. DeMuth, Amphiphile–CpG vaccination induces potent lymph node activation and COVID-19 immunity in mice and non-human primates. *NPI Vaccines* **7**, 128 (2022).
28. S. Pant, Z. A. Wainberg, C. D. Weekes, M. Furqan, P. M. Kasi, C. E. Devoe, A. D. Leal, V. Chung, O. Basturk, H. VanWyk, A. M. Tavares, L. M. Seenappa, J. R. Perry, T. Kheoh, L. K. McNeil, E. Welkowsky, P. C. DeMuth, C. M. Haqq, E. M. O'Reilly, Lymph-node-targeted, mKRAS-specific amphiphile vaccine in pancreatic and colorectal cancer: the phase 1 AMPLIFY-201 trial. *Nat. Med.* **30**, 531–542 (2024).
29. Z. A. Wainberg, C. D. Weekes, M. Furqan, P. M. Kasi, C. E. Devoe, A. D. Leal, V. Chung, J. R. Perry, T. Kheoh, L. K. McNeil, E. Welkowsky, P. C. DeMuth, C. M. Haqq, S. Pant, E. M. O'Reilly, Lymph node–targeted, mKRAS-specific amphiphile vaccine in pancreatic and colorectal cancer: Phase 1 AMPLIFY-201 trial final results. *Nat. Med.* **31**, 3648–3653 (2025).
30. S. Iurescia, D. Fioretti, M. Rinaldi, Nucleic acid sensing machinery: Targeting innate immune system for cancer therapy. *Recent Pat. Anticancer Drug Discov.* **13**, 2–17 (2018).
31. C. Vanpouille-Box, J. A. Hoffmann, L. Galluzzi, Pharmacological modulation of nucleic acid sensors—Therapeutic potential and persisting obstacles. *Nat. Rev. Drug Discov.* **18**, 845–867 (2019).
32. L. Unterholzner, S. E. Keating, M. Baran, K. A. Horan, S. B. Jensen, S. Sharma, C. M. Sirois, T. Jin, E. Latz, T. S. Xiao, K. A. Fitzgerald, S. R. Paludan, A. G. Bowie, IFI16 is an innate immune sensor for intracellular DNA. *Nat. Immunol.* **11**, 997–1004 (2010).
33. J. R. Nakkala, Y. Li, L. Akter, X. Kang, X. Chen, Differential regulation of DC function, adaptive immunity, and MyD88 dependence by MF59 and AS03-like adjuvants. *Vaccines* **12**, 531 (2024).
34. R. M. Martin, J. L. Brady, A. M. Lew, The need for IgG2c specific antiserum when isotyping antibodies from C57BL/6 and NOD mice. *J. Immunol. Methods* **212**, 187–192 (1998).
35. A. M. Collins, IgG subclass co-expression brings harmony to the quartet model of murine IgG function. *Immunol. Cell Biol.* **94**, 949–954 (2016).
36. M. B. Furtess, S.-R. Woo, B. Burnett, Y.-X. Fu, T. F. Gajewski, Type I interferon response and innate immune sensing of cancer. *Trends Immunol.* **34**, 67–73 (2013).
37. B. Briard, D. E. Place, T.-D. Kanneganti, DNA sensing in the innate immune response. *Physiology* **35**, 112–124 (2020).
38. H. Häcker, P.-H. Tseng, M. Karin, Expanding TRAF function: TRAF3 as a tri-faced immune regulator. *Nat. Rev. Immunol.* **11**, 457–468 (2011).
39. D. Ori, M. Murase, T. Kawai, Cytosolic nucleic acid sensors and innate immune regulation. *Int. Rev. Immunol.* **36**, 74–88 (2017).
40. S. Liu, X. Cai, J. Wu, Q. Cong, X. Chen, T. Li, F. Du, J. Ren, Y. T. Wu, N. V. Grishin, Z. J. Chen, Phosphorylation of innate immune adaptor proteins MAVS, STING, and TRIF induces IRF3 activation. *Science* **347**, aaa2630 (2015).
41. M. Lin, X. Ji, Y. Lv, D. Cui, J. Xie, The roles of TRAF3 in immune responses. *Dis. Markers* **2023**, 7787803 (2023).
42. B. L. Lee, J. E. Moon, J. H. Shu, L. Yuan, Z. R. Newman, R. Schekman, G. M. Barton, UNC93B1 mediates differential trafficking of endosomal TLRs. *eLife* **2**, e00291 (2013).
43. A. Casrouge, S.-Y. Zhang, C. Eidenschenk, E. Jouanguy, A. Puel, K. Yang, A. Alcais, C. Picard, N. Mahfoufi, N. Nicolas, L. Lorenzo, S. Plancoulaine, B. Sénéchal, F. Geissmann, K. Tabeta, K. Hoebe, X. Du, R. L. Miller, B. Héron, C. Mignot, T. B. de Villemeur, P. Lebon, O. Dulac, F. Rozenberg, B. Beutler, M. Tardieu, L. Abel, J.-L. Casanova, Herpes simplex virus encephalitis in human UNC-93B deficiency. *Science* **314**, 308–312 (2006).
44. B. Donaldson, Z. Lateef, G. F. Walker, S. L. Young, V. K. Ward, Virus-like particle vaccines: Immunology and formulation for clinical translation. *Expert Rev. Vaccines* **17**, 833–849 (2018).
45. R. Kensinger, A. B. Arunachalam, Preclinical development of the quadrivalent meningococcal (ACYW) tetanus toxoid conjugate vaccine, MenQuadfi. *Glycoconj. J.* **39**, 381–392 (2022).
46. M. Ledwith, Pneumococcal conjugate vaccine. *Curr. Opin. Pediatr.* **13**, 70–74 (2001).
47. A. Papi, M. G. Ison, J. M. Langley, D.-G. Lee, I. Leroux-Roels, F. Martinon-Torres, T. F. Schwarz, R. N. van Zyl-Smit, L. Campora, N. Dezutter, N. de Schrevel, L. Fissette, M.-P. David, M. Van der Wielen, L. Kostanyan, V. Hulström, Respiratory syncytial virus prevention F protein vaccine in older adults. *N. Engl. J. Med.* **388**, 595–608 (2023).
48. C. L. White, M. A. Glover, S. K. Gandhapudi, K. A. Richards, A. J. Sant, Flublok quadrivalent vaccine adjuvanted with R-DOTAP elicits a robust and multifunctional CD4 T cell response that is of greater magnitude and functional diversity than conventional adjuvant systems. *Vaccine* **12**, 281 (2024).
49. J. M. Curtsinger, J. O. Valenzuela, P. Agarwal, D. Lins, M. F. Mescher, Cutting edge: Type I IFNs provide a third signal to CD8 T cells to stimulate clonal expansion and differentiation. *J. Immunol.* **174**, 4465–4469 (2005).
50. G. A. Kolumam, S. Thomas, L. J. Thompson, J. Sprent, K. Murali-Krishna, Type I interferons act directly on CD8 T cells to allow clonal expansion and memory formation in response to viral infection. *J. Exp. Med.* **202**, 637–650 (2005).
51. W. Lee, M. Suresh, Vaccine adjuvants to engage the cross-presentation pathway. *Front. Immunol.* **13**, 940047 (2022).
52. D. J. Drakes, A. M. Abbas, J. Shields, M. P. Steinbuck, A. Jakubowski, L. M. Seenappa, C. M. Haqq, P. C. DeMuth, Lymph node–targeted vaccine boosting of TCR T-cell therapy enhances antitumor function and eradicates solid tumors. *Cancer Immunol. Res.* **12**, 214–231 (2024).
53. V. Dasari, L. K. McNeil, K. Beckett, M. Solomon, G. Ambalathingal, T. Le Thuy, A. Panikkar, C. Smith, M. P. Steinbuck, A. Jakubowski, L. M. Seenappa, E. Palmer, J. Zhang, C. M. Haqq, P. C. DeMuth, R. Khanna, Lymph node targeted multi-epitope subunit vaccine promotes effective immunity to EBV in HLA-expressing mice. *Nat. Commun.* **14**, 4371 (2023).
54. G. A. F. Vitiello, W. A. S. Ferreira, V. C. Cordeiro de Lima, T. da Silva Medina, Antiviral responses in cancer: Boosting antitumor immunity through activation of interferon pathway in the tumor microenvironment. *Front. Immunol.* **12**, 782852 (2021).
55. S. A. Plotkin, Updates on immunologic correlates of vaccine-induced protection. *Vaccine* **38**, 2250–2257 (2020).
56. I. Kudryavtsev, Y. Zinchenko, M. Serebriakova, T. Akisheva, A. Rubinsteyn, A. Savchenko, A. Borisov, V. Belenjuk, A. Malkova, P. Yablonskiy, D. Kudlay, A. Starshinova, A key role of CD8<sup>+</sup> T cells in controlling of tuberculosis infection. *Diagnostics* **13**, 1–15 (2023).
57. M. B. B. McCall, P. G. Kremsner, B. Mordmüller, Correlating efficacy and immunogenicity in malaria vaccine trials. *Semin. Immunol.* **39**, 52–64 (2018).
58. V. Torchilin, Intracellular delivery of protein and peptide therapeutics. *Drug Discov. Today Technol.* **5**, e95–e103 (2008).
59. B. Winkeljann, D. C. Keul, O. M. Merkel, Engineering poly- and micelleplexes for nucleic acid delivery—A reflection on their endosomal escape. *J. Control. Release* **353**, 518–534 (2023).
60. N. Petrovsky, J. C. Aguilar, Vaccine adjuvants: Current state and future trends. *Immunol. Cell Biol.* **82**, 488–496 (2004).
61. C. Maisonneuve, S. Bertholet, D. J. Philpott, E. De Gregorio, Unleashing the potential of NOD- and Toll-like agonists as vaccine adjuvants. *PNAS* **111**, 12294–12299 (2014).
62. I. J. Amanna, M. K. Sifka, Contributions of humoral and cellular immunity to vaccine-induced protection in humans. *Virology* **411**, 206–215 (2011).
63. M. Choteau, A. Scohy, S. Messe, M. Luycckx, M. Dechamps, V. Montiel, J. C. Yombi, D. Gruson, N. Limaye, T. Michiels, L. Dumoutier, Development of SARS-CoV2 humoral response including neutralizing antibodies is not sufficient to protect patients against fatal infection. *Sci. Rep.* **12**, 2077 (2022).

64. D. R. Feikin, M. M. Higdon, L. J. Abu-Raddad, N. Andrews, R. Araos, Y. Goldberg, M. J. Groome, A. Huppert, K. L. O'Brien, P. G. Smith, A. Wilder-Smith, S. Zeger, M. Deloria Knoll, M. K. Patel, Duration of effectiveness of vaccines against SARS-CoV-2 infection and COVID-19 disease: Results of a systematic review and meta-regression. *Lancet* **399**, 924–944 (2022).
65. F. Menegale, M. Manica, A. Zardini, G. Guzzetta, V. Marziano, V. d'Andrea, F. Trentini, M. Ajelli, P. Poletti, S. Merler, Evaluation of waning of SARS-CoV-2 vaccine-induced immunity: A systematic review and meta-analysis. *JAMA Netw. Open* **6**, e2310650 (2023).
66. S. Xu, J. Li, H. Wang, F. Wang, Z. Yin, Z. Wang, Real-world effectiveness and factors associated with effectiveness of inactivated SARS-CoV-2 vaccines: A systematic review and meta-regression analysis. *BMC Med.* **21**, 160 (2023).
67. F. Spadaro, C. Lapenta, S. Donati, L. Abalsamo, V. Barnaba, F. Belardelli, S. M. Santini, M. Ferrantini, IFN- $\alpha$  enhances cross-presentation in human dendritic cells by modulating antigen survival, endocytic routing, and processing. *Blood* **119**, 1407–1417 (2012).
68. L. Lattanzi, C. Roza, D. Marescotti, G. D'Agostino, L. Santodonato, S. Cellini, F. Belardelli, R. Gavioli, M. Ferrantini, IFN- $\alpha$  boosts epitope cross-presentation by dendritic cells via modulation of proteasome activity. *Immunobiology* **216**, 537–547 (2011).
69. N. Zagorulya, S. Spranger, Once upon a prime: DCs shape cancer immunity. *Trends Cancer* **9**, 172–184 (2023).
70. L. Shen, L. J. Sigal, M. Boes, K. L. Rock, Important role of cathepsin S in generating peptides for TAP-independent MHC class I crosspresentation in vivo. *Immunity* **21**, 155–165 (2004).
71. R. J. Riese, R. N. Mitchell, J. A. Villadangos, G. P. Shi, J. T. Palmer, E. R. Karp, G. T. De Sanctis, H. L. Ploegh, H. A. Chapman, Cathepsin S activity regulates antigen presentation and immunity. *J. Clin. Invest.* **101**, 2351–2363 (1998).
72. V. Hornung, S. Rothenfusser, S. Britsch, A. Krug, B. Jahrsdörfer, T. Giese, S. Endres, G. Hartmann, Quantitative expression of Toll-like receptor 1–10 mRNA in cellular subsets of human peripheral blood mononuclear cells and sensitivity to CpG oligodeoxynucleotides. *J. Immunol.* **168**, 4531–4537 (2002).
73. N. Kadowaki, S. Ho, S. Antonenko, R. de Waal Malefyt, R. A. Kastelein, F. Bazan, Y.-J. Liu, Subsets of human dendritic cell precursors express different Toll-like receptors and respond to different microbial antigens. *J. Exp. Med.* **194**, 863–870 (2001).
74. J. Ahn, D. Gutman, S. Saijo, G. N. Barber, STING manifests self DNA-dependent inflammatory disease. *Proc. Natl. Acad. Sci. U.S.A.* **109**, 19386–19391 (2012).
75. D. M. Valenzuela, A. J. Murphy, D. Frendewey, N. W. Gale, A. N. Economides, W. Auerbach, W. T. Poueymirou, N. C. Adams, J. Rojas, J. Yasenchak, R. Chernomorsky, M. Boucher, A. L. Elsassser, L. Esau, J. Zheng, J. A. Griffiths, X. Wang, H. Su, Y. Xue, M. G. Dominguez, I. Noguera, R. Torres, L. E. Macdonald, A. F. Stewart, T. M. DeChiara, G. D. Yancopoulos, High-throughput engineering of the mouse genome coupled with high-resolution expression analysis. *Nat. Biotechnol.* **21**, 652–659 (2003).
76. Q. Sun, L. Sun, H.-H. Liu, X. Chen, R. B. Seth, J. Forman, Z. J. Chen, The specific and essential role of MAVS in antiviral innate immune responses. *Immunity* **24**, 633–642 (2006).
77. J. W. Jones, N. Kayagaki, P. Broz, T. Henry, K. Newton, K. O'Rourke, S. Chan, J. Dong, Y. Qu, M. Roose-Girma, V. M. Dixit, D. M. Monack, Absent in melanoma 2 is required for innate immune recognition of *Francisella tularensis*. *Proc. Natl. Acad. Sci. U.S.A.* **107**, 9771–9776 (2010).
78. H. Hemmi, O. Takeuchi, T. Kawai, T. Kaisho, S. Sato, H. Sanjo, M. Matsumoto, K. Hoshino, H. Wagner, K. Takeda, S. Akira, A Toll-like receptor recognizes bacterial DNA. *Nature* **408**, 740–745 (2000).

**Acknowledgments:** We thank C. Carter, J. Fontenot, and F. Villinger at New Iberia Research Center for the execution of the NHP studies; the NIH Tetramer Core Facility at Emory University (NIH contract 75N93020D00005 and RRID:SCR\_026557) for supplying the SARS-CoV-2 RBD tetramer; and D. J. Irvine at the Massachusetts Institute of Technology/Scripps Research Institute for helpful advice and discussion. **Funding:** Research conducted at Elicio Therapeutics was funded by Elicio Therapeutics. Research conducted at the University of Massachusetts was supported by the UMass Chan School Fund NIH/NHLBI 5R01 HL165787. **Author contributions:** Conceptualization: M.P.S., W.Z., L.K.M., K.A.F., and P.C.D. Methodology: M.P.S., W.Z., A.J., L.K.M., K.A.F., and P.C.D. Investigation: M.P.S., L.M.S., W.Z., E.P., M.M.J., A.J., X.C.-P., and L.K.M. Data curation: M.P.S. and L.K.M. Formal analysis: M.P.S., L.M.S., W.Z., M.M.J., A.J., X.C.-P., L.K.M., K.A.F., and P.C.D. Validation: M.P.S., L.M.S., W.Z., M.M.J., L.K.M., and K.A.F. Visualization: M.P.S., W.Z., L.K.M., K.A.F., and P.C.D. Supervision: M.P.S., C.M.H., K.A.F., and P.C.D. Writing—original draft: M.P.S. Writing—review and editing: M.P.S., W.Z., M.M.J., X.C.-P., L.K.M., C.M.H., K.A.F., and P.C.D. Resources: L.M.S., M.M.J., and K.A.F. Funding acquisition: C.M.H., K.A.F., and P.C.D. Project administration: M.P.S., K.A.F., and P.C.D. **Competing interests:** M.P.S., E.P., X.C.-P., M.M.J., L.K.M., C.M.H., and P.C.D. are employees and equity holders of Elicio Therapeutics, Inc. M.P.S. and P.C.D. are inventors on a pending patent application covering the AMP-DNA adjuvants (18/684,014). Patents have been filed by Elicio Therapeutics, Inc. on 15 August 2022. The other authors declare that they have no competing interests. **Data, code, and materials availability:** All data and code needed to evaluate and reproduce the results in the paper are present in the paper, the Supplementary Materials, and/or public repositories. NanoString data are available in the Gene Expression Omnibus (GEO) under accession numbers GSE280859 (ncbi.nlm.nih.gov/geo/query/acc.cgi?acc=GSE280859) and GSE280856 (ncbi.nlm.nih.gov/geo/query/acc.cgi?acc=GSE280856) for the mouse and NHP data sets, respectively. Details for how to synthesize materials are provided in Materials and Methods.

Submitted 9 September 2025

Accepted 17 April 2026

Published 29 May 2026

10.1126/sciadv.aec1416

## Lymph node–targeted DNA engages TBK1/IFN-I–driven innate immunity to induce potent T cell responses and durable memory in mice and NHPs

Martin P. Steinbuck, Lochana M. Seenappa, Wei Zhan, Erica Palmer, Mimi M. Jung, Aniela Jakubowski, Xavier Cabana-Puig, Lisa K. McNeil, Christopher M. Haqq, Katherine A. Fitzgerald, and Peter C. DeMuth

*Sci. Adv.* **12** (22), eaec1416. DOI: 10.1126/sciadv.aec1416

### View the article online

<https://www.science.org/doi/10.1126/sciadv.aec1416>

### Permissions

<https://www.science.org/help/reprints-and-permissions>

Use of this article is subject to the [Terms of service](#)

---

*Science Advances* (ISSN 2375-2548) is published by the American Association for the Advancement of Science, 1200 New York Avenue NW, Washington, DC 20005. The title *Science Advances* is a registered trademark of AAAS.

Copyright © 2026 The Authors, some rights reserved; exclusive licensee American Association for the Advancement of Science. No claim to original U.S. Government Works. Distributed under a Creative Commons Attribution NonCommercial License 4.0 (CC BY-NC).